A Molecular Dynamics Simulation of Vesicle Deformation and Rupture in Confined Poiseuille Flow

by

Alison Harman

Thesis submitted to the

Faculty of Graduate and Postdoctoral Studies

In partial fulfillment of the requirements

For the M.Sc. degree in

Physics

Department of Physics

Faculty of Science

University of Ottawa

Abstract

Vesicles are simple structures, but display complex, non-linear dynamics in fluid flow. I investigate the deformation of nanometer-sized vesicles, both fully-inflated and those with excess area, as they travel in tightly confined capillaries. By varying both channel size and flow strength, I simulate vesicles as they transition from steady-state to unstable shapes, and then rupture in strong flow fields. By employing a molecular dynamics model of the vesicle, fluid, and capillary system one is able to rupture the lipid bilayer of these vesicles. This is unique in that most other numerical methods for modelling vesicles are unable to show rupture. The rupture of fully-inflated vesicles is applicable to drug delivery in which the release of the encapsulated medicine needs to be controlled. The deformation and rupture of vesicles with excess area could be applicable to red blood cells which have similar rheological properties.

Acknowledgements

I would like to thank my supervisor, Dr. Béla Joós, for giving me the opportunity to pursue further education and research at the wonderful University of Ottawa. It is a privilege to interact with the talented and exciting research community at the university. I would also like to thank Dr. Joós for his encouragement through our group meetings and providing the opportunity to interact with the larger research community at the American Physical Society meeting in March 2012. A special thanks to Martin Bertrand for his direction on this project. His enthusiasm, his time spent setting up my computer for the subsequent simulation and analysis, and his ideas are always appreciated. I would also thank my office mates, Ben Barlow and Louis Jacques, for their ideas, technical help, and companionship. On a more personal note, I would like to thank my partner, Kevin, for his unfailing support.

Contents

List of Tables

List of Figures

Chapter 1

Introduction

Vesicles are simple mechanical analogues to cells, in particular red blood cells (RBCs). They have the same lipid bilayer as cells, but lack the more complicated features of cells (such as embedded proteins in the bilayer, complex cytoplasm, the internal structure provided by the cytoskeleton, etc.). Vesicles in fluid flow can display complex, non-linear dynamics which are often modelled using numerical techniques. This thesis explores the suitability of a Coarse-Grained Molecular Dynamics (CGMD) simulation as a method for modelling vesicles in Poiseuille flow (i.e. flow through a tube) and how vesicles rupture in strong flow fields. (Molecular Dynamics (MD) is type of numerical integration in which particle interaction is governed through mean fields. Coarse-Grained mean that the particles in the simulation are not of atomistic (realistic) detail, but are instead represented by conglomerate particles, e.g. our polar head-groups are represented as one particle.) A picture of our MD simulation can be seen in Figure 1.1.

The study of rupture is unique compared to other numerical methods of modelling vesicles in fluid flow, which assume the bilayer is an impenetrable surface. I use a simple model of a vesicle in which one type of lipid composes the bilayer and the internal fluid of the vesicle is the same as the external fluid. The radius of the capillary and the strength

of the fluid flow can be varied while the vesicle remains the same. Both a decreased radius of the capillary and an increased fluid flow strength increase the stress imposed on the vesicle.

1.1 Motivation

Vesicles make great experimental subjects as they have a few key parameters that define them and these can be varied, which allows for studies, both theoretical and experimental. These parameters include the elastic constant of the membrane, excess area (or, equivalently, reduced volume), and viscosity of the internal fluid. The elastic constant of the membrane is determined by the type of lipids composing the membrane. As a real-life example, more cholesterol in a membrane increases packing order and reduces the elasticity of the membrane. Excess area refers to the surface area of the membrane as compared to the enclosed internal volume. For a spherical, fully-inflated vesicle, the excess area is defined to be zero. If the surface area is larger than the surface area of a sphere (that encloses a set volume), the excess area is greater than zero. Vesicles with large excess areas are "floppy" and more deformable as they enclose a small volume to surface area.

There are several reasons to study vesicles besides their simplicity in structure. Vesicles are manufactured for medical, biological, and experimental purposes and are often known as liposomes in this context. Liposomes can be designed as drug-delivery vehicles in which the therapeutic agent is enclosed in the interior of the vesicle. The liposomes can then be injected into a vascular system of animals or humans and often collect at sites of inflammation or tumour sites [34]. The rupture of liposomes is key to their function. My study of the rupture of fully-inflated vesicles in confined channels could be applicable to drug-delivery. For instance, in cases of ischemia there is a constriction in blood flow and the rupture of liposomes due to confinement could be applicable. Indeed there have

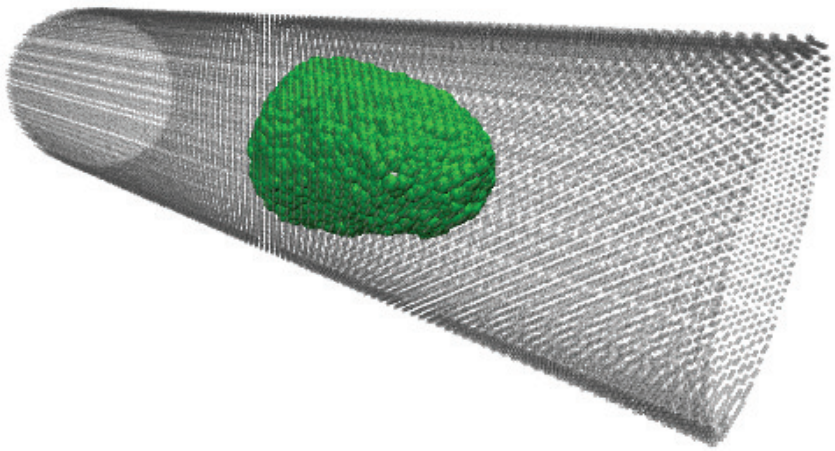

Figure 1.1: My 3D model of a vesicle (in green) flowing through the centre of a capillary. The fluid inside the capillary is not shown. The green spheres composing the vesicle represent the polar head groups of the lipids. The capillary is also shown and the particles (or beads) comprising its structure can be seen as well.

already been several liposomal-enclosed medicines that have been applied in the case of ischemia of the brain (such as in the case of stroke) [53], [61] and of the heart (as in the case of atheroscherosis) [57].

My molecular dynamics simulation as represented in Figure 1.1 is analogous to microfluidics setups in which there is a controlled environment in which small amount of particles can be manipulated. My simulation provides a virtual laboratory in which many experiments could be performed, such as varying the properties of the vesicle or the channel. A molecular dynamics simulation can relatively easy to adapted to specific channel configurations; an example would be a saw-tooth channel wall rather than a smooth one. The main issue with a molecular dynamics simulation is that there are size limitations to the systems that can be simulated. If the channel radius is doubled, the number of particles to be simulated quadruples. This necessitates the simulation of small vesicles and small capillaries. My vesicle has three thousand lipids and its bilayer thickness is comparable to its diameter which means that my vesicle is nanometer-sized object. This is based on the fact that the bilayer thickness is around five nanometers.

The other major reason to study vesicles is their rheological similarity to "simpler" cells such as red blood cells (RBCs) and platelets. The deformation of vesicles and RBCs is quite similar in Poiseuille flow and, as such, the study of vesicles is used as an insight into the behaviour of RBCs. RBCs have a large excess area and this floppiness helps them to transverse narrow corridors in which the radii of RBCs and the microvasculature are of a similar length. (Excess area will be formally defined in the next chapter. Excess area means that there is a larger amount of surface area compared to a sphere enclosing the same internal volume of the RBC.) The large deformability of this membrane makes numerical calculations of its configuration (especially in three dimensions) in fluid flow more difficult than fully-inflated vesicles. It is a challenge to solve for fluid forces on a very deformable membrane, but has been done using numerical approaches. Our MD

simulation provides another way to simulate these dynamics. Our results for floppy vesicles, with excess area of five (the same excess area as RBCs), are compared to other simulation work in this thesis.

The most significant structural difference between RBCs and vesicles is that vesicles lack a cytoskeleton (which can provide extra resistance to stretching). The rupture of my vesicles with excess area may not be applicable to RBCs as a cytoskeleton may prevent the large deformations seen in my vesicles. However, there are very few papers that detail the rupture of red blood cells in the context of Poiseuille flow so my study of the rupture of vesicles with excess area should be of interest to the topic of hemolysis (red blood cell rupture).

1.2 Goals and Objectives

The first goal of this thesis is to compare our simulation results to experimental data in a quantifiable way. There is a study of the deformation of nearly fully-inflated vesicles done by Vitkova *et al.* [58]. The shape deformations of their vesicles and my vesicle are similar despite a two order-of-magnitude difference in radii. This provides confidence that our MD model of vesicle and capillary provides sensible results in regards to shape deformation.

Another objective of this work is to analyze the shape deformation and tension in the bilayer while varying flow strength, confinement of the vesicle within the capillary, and excess area. Shape deformation of vesicles in these contexts is still a current area of research. I map the tension (as determined by the area expansion of the lipids) onto to these vesicle shapes. This is unique as generally the tension is not shown in other works. The build-up of tension in a bilayer (as flow strength increases) is where rupture usually occurs. Modelling the rupture of vesicles is also unique as most theoretical and numerical techniques assume a continuous surface.

1.3 Contributions

The main contribution of this thesis is the study of vesicle rupture. The time-scale at which rupture occurs is very fast and there are no experimental studies of the rupture of vesicles in Poiseuille flow. It is possible that this study of rupture when published will provoke some experiments to capture this phenomenon. Also, it is possible that the study of rupture and confinement will inspire new liposomal medicines which could treat conditions in which there is constrained blood flow, such as stroke, atherosclerosis, diabetes, or gangrene.

In addition, a CGMD simulation could be an efficient, simple way to model the shape deformation of vesicles with large excess areas. In particular, it is time-consuming to analyze the shape deformation of these vesicles in three dimensions. Our CGMD simulation addresses this issue as using Graphical Processing Units (GPUs) can perform similar calculations simultaneously. GPUs are employed in the gaming industry in which this ability is highly useful for high-speed graphics processing. This means that powerful, gaming GPUs can be obtained at low cost for high computing power which then can be used to study vesicle dynamics.

1.4 Summary

The next chapter introduces some key concepts such as excess area and the Helfrich Hamiltonian necessary to understand the rest of the thesis. Also included in that chapter is a review of the current research on the topic of vesicles in Poiseuille flow. The third chapter reveals the detail of the molecular dynamic simulation parameters and a summary of data analysis techniques used. The fourth chapter contains all the results of these simulations and discussions of the results. The concluding chapter summaries the calculations, talks about open issues, and possible improvements to the model.

Chapter 2

Key Concepts and Current Research in the Field

Since I am often asked "What is biophysics?", I will give a brief introduction to the subject. Biophysics (or equivalently biological physics) is an interdisciplinary field in which researchers can come from several departments such as molecular biology, biochemistry, computer science, mathematics, medicine, and physics. Since the mid-1990s it has been a growing field of research, often with the work done by physicists who had been working in traditional sub-fields of physics. Techniques employed include: physical techniques such as atomic force microscopy (AFM) and optical tweezers; computational techniques such as molecular dynamics; and imaging techniques such as fluorescent imaging, NMR spectroscopy, and x-ray crystallography. Complex biological events are then understood through physical theories such as statistical mechanics, thermodynamics, and chemical kinetics.

Biophysics is the application of concepts and techniques from physics to problems in biology. These problems span all levels of biological organization from molecular scales, to cells, to organisms, to ecosystems. A good introductory book in this field is

Philip Nelson's *Biological Physics* [44]; in this book basic concepts such as free energy, entropy, random walks, etc. are shown to have applicability when trying to understand the micron-sized world of cells, bacteria, proteins, etc.. Another good introductory book which is more detailed with an emphasis on a statistical mechanical analysis and focuses on cells in particular is Rob Phillips' *Physical Biology of the Cell* [48]. The goal of biophysics is to understand simple mechanical basis underlying the complexity seen in biology and to have a quantitative basis on which to understand biological phenomenon.

2.1 Introduction to Vesicles

Vesicles are self-assembled objects which consist of a bilayer membrane (like cells), but lack the other more complex features of cells such as a complex internal cytoplasm, a nucleus, or a cytoskeleton. The stability of both vesicles and cells are dependent on the hydrophobic effect. As lipids consist of a hydrophilic (water-loving) head and a hydrophobic (water-fearing) tail, the energy of the system can be minimized when the tails face each other rather than the water. This means that lipids of the right geometry can self-assemble into a lipid bilayer. In a bilayer configuration, the ends of the bilayer are still exposed to the water which increases the free energy of the system. So, even though there is an energy associated with the bending of a lipid bilayer, the ends of the bilayer can connect to form a vesicle. A vesicle therefore is a self-contained object which has an interior fluid which may or may not be different than the external fluid. The various structures of lipid, bilayer, and vesicle can be seen in Figure 2.1.

As vesicles act as little containers of fluids, they are often found in cells as transport mechanisms and/or as storage containers. As an example of intracellular transport, vesicles can move proteins from the rough endoplasmic reticulum to the Golgi apparatus. They can also be used as excretory vehicles. In this case, vesicles can fuse with the cellular lipid bilayer membrane and excrete substances ranging from enzymes to waste products.

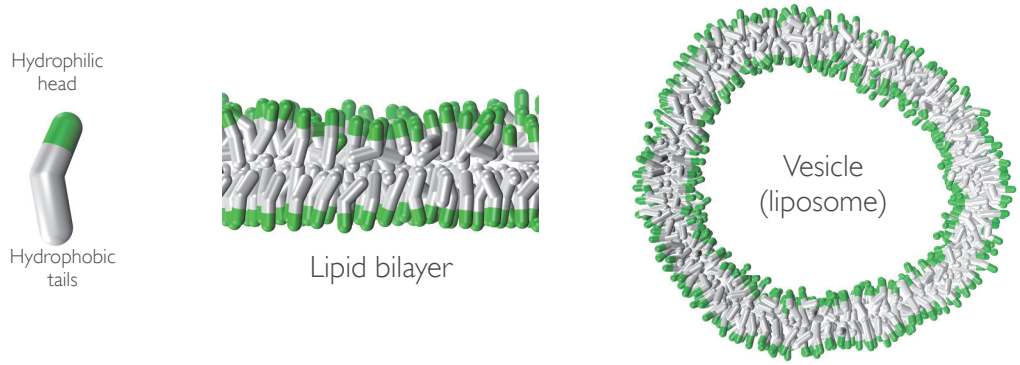

Figure 2.1: A coarse-grained model of lipids in which the heads are represented by green and the tails in white. A section of bilayer is shown as well as a cross-sectional view of a vesicle or liposome.

Intracellular vesicles are very small, being of the submicron scale.

Vesicles can also be manufactured in labs and in this context they are often known as *liposomes*. One technique that can manufacture them is electroformation [43]. In this case, a dry lipid film is applied to indium tin oxide (ITO) coated glass plates which is then placed in an aqueous solution. An AC voltage is applied to the chamber containing the glass plates and solution. The electric field parameters (the voltage and the frequency) guide vesicle growth. In this manner, giant unilamellar vesicles (GUVs) are produced; they range from 5 to 200 μm in diameter. Through this technique one can choose the lipid type or types which compose the vesicle and also choose the internal solution of the vesicle. To produce small unilamellar vesicles (SUVs), one can extrude GUVs through nano-channel arrays. In this manner, smaller vesicles can be produced. Nano-sized vesicles ($\sim$ 100 nm) are often used as drug-delivery systems due to their greater stability than GUVs [24].

Since vesicles have the same outer bilayer as cell and membrane-bound organelles do, their potential for use in biomedical applications as been long realized. In fact there are

already licensed medicines approved for use, including liposome-based vaccines [25], and new uses and technologies are still being developed including applications such as gene delivery [5]. Vesicle use in nanotechnologies such as miniature "bioreactors" is also being investigated [46], [35].

GUVs also mimic some of the dynamics of red blood cells (RBCs), such as their equilibrium biconcave shape. As such, they are studied intensively as simple mechanical models from which to gain insight into red blood cell dynamics. Since GUVs are fairly large objects relatively speaking, individual GUVs can be manipulated and observed in real time with optical microscopy [58].

Since vesicles are much simpler than cells, there are few key parameters that define them. This makes them easier test subjects for theoretical and numerical studies than RBCs and can give insight into the mechanical aspects of cell behaviour. While cells have the same lipid bilayer as vesicles, they are composed of different types of lipids and often the composition of the inner layer of lipids or leaflet is different from the outer leaflet. Cells also have a much more complex internal environment than manufactured vesicles. For instance, the interior consists of an inhomogeneous cytoplasm, several different organelles, a cytoskeleton, and often a nucleus. Red blood cells are one of the simpler types of cells as they do not contain organelles and do not have a nucleus. Nevertheless, vesicles and RBCs adopt similar shapes in Poiseuille flow. The few key parameters that define vesicles are the viscosity of the filling fluid, volume-to-surface ratio, and the diameter.

While the viscosity of the filling fluid can be different than external fluid, for most of the theoretical and experimental studies the ratio of the external to the internal fluid is one. In other words, the same fluid is outside and inside the vesicle. Although as external fluid viscosity increases relative to the internal fluid viscosity the vesicle will be less deformable and behave more like a solid spherical particle. For simplicity, my simulation model uses the same fluid outside and inside the vesicle.

The volume-to-surface ratio is perhaps one the more interesting parameters that one can vary. Stable shapes of quiescent vesicles are largely determined by the volume-to-surface ratio [51]. If both the internal fluid volume and the surface area are the equivalent the volume and surface area of spheres respectively, then the vesicle is fully-inflated. Otherwise if the surface area of the sphere is greater than the surface area of a sphere enclosing the internal volume of the vesicle, then the vesicle is partially "deflated" and much more deformable; the surface area to internal volume ratio is greater. This concept is defined mathematically by the *excess area* or equivalently the *reduced volume* of a vesicle. To define the excess area, first the nominal radius of a vesicle is defined as $R_0 = (3V/4\pi)^{1/3}$ where V is the volume of the vesicle. This definition of R_0 allows one to define the excess area of a vesicle. The excess area is the difference between the vesicle area and area of an equivalent sphere:

$$\Delta = \frac{A}{R_0^2} - 4\pi \tag{2.1}$$

$\Delta = 0$ for a sphere, and $\Delta > 0$ otherwise and A is the surface area of the vesicle. For RBCs Δ is around 5 which means that the membranes are easily deformable as they have large surface area compared to their enclosed volume. This deformability is a feature that enables them to traverse narrow capillaries without breaking or becoming blocked.

An equivalent term is reduced volume. In this case $R_0 = \sqrt{A/4\pi}$ and its reduced volume is given as:

$$\nu = \frac{V}{4/3\pi R_0^3} \tag{2.2}$$

$\nu = 1.0$ for fully inflated vesicles and for RBCs $\nu = 0.6$. In this thesis I will use both the terms, *excess area* and *reduced volume*, interchangeably.

The diameter of the vesicle is another important parameter. In the case of GUVs, the diameter is two orders of magnitude greater than the thickness of the bilayer, which is around $5nm$. In this case, the surface can be considered a 2D surface as the thickness of the bilayer is negligible. Most theoretical studies use this assumption when studying the

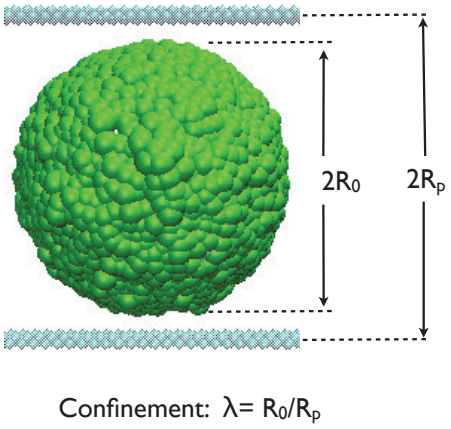

Figure 2.2: A fully-inflated vesicle in its initial configuration before fluid forces are applied. Confinement will be referred to frequently in this thesis and is defined as the initial radius of the vesicle R_0, to the radius of the capillary (sometimes called a pore), R_p.

theoretical behaviour of vesicles such as equilibrium shapes or shape changes under fluid flow. As will be seen, this is not possible with our Molecular Dynamics (MD) simulation of the vesicle as the thickness of our bilayer is comparable to the overall dimensions of the vesicle.

An important parameter when studying vesicles under fluid flow is the ratio of the tube or channel enclosing the vesicle and the diameter of the vesicle. As this thesis will be studying closely confined vesicles (i.e. where the ratio is close to one) this will strongly effect vesicle shapes obtained and the eventual rupture of the vesicles. The ratio is defined as:

$$\lambda = \frac{R_0}{R_p} \tag{2.3}$$

where R_p is the radius of the pore or capillary and can be seen in Figure 2.2.

2.2 Area Compressibility and Bending Modulus

The concepts of stretching and bending can be understood from the analysis of stretching and bending of one-dimensional beams or sheets [48]. This simple underlying theory can be applied to such things in the living sub-micron world as the cytoskeleton of a cell, stereocilia which vibrate to sound in the human ear, or flagella that propel cells [15]. The concepts of stretching and bending can also be easily applied to two-dimensional membranes as will be shown.

If one has a planar, lipid membrane at its preferred area per lipid head, a_0, then energy cost to stretch this membrane by some change in area per lipid, Δa, can be written as a series expansion:

$$E_{stretch} = C_0 + C_1 \Delta a + C_2 (\Delta a)^2 + ... \tag{2.4}$$

where C_0, C_1, and C_2 are constants. C_0 is an arbitrary constant and can be set to zero. C_1 is equal to zero since membranes behave like springs in that the energy is proportional to the square of the deformation. Therefore to lowest order one can write the energy change as

$$E_{stretch} = \frac{1}{2} K_A \frac{(A - A_0)^2}{A_0} \tag{2.5}$$

where K_A is defined to be the proportionality constant. The above equation could have been written as:

$$E_{stretch} = \frac{1}{2} \tilde{K}_A (A - A_0)^2 \tag{2.6}$$

where $\tilde{K}_A = K_A / A_0$. However the definition of K_A from equation 2.5, enables one to write the below equation

$$\sum \equiv \frac{\delta E_{stretch}}{\delta A} = K_A \frac{A - A_0}{A_0} = K_A \alpha \tag{2.7}$$

in which $\sum$ is the tension (lateral stress) in the membrane and α is the dimensional strain. Thus stress is proportional to strain and Hooke's law has been recovered. K_A is known as the *area compressibility modulus*.

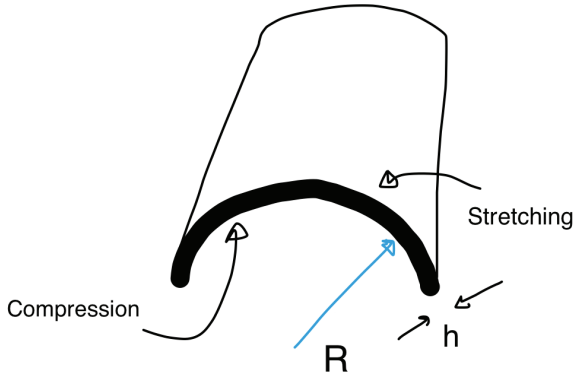

Figure 2.3: The bending of a sheet of thickness h with radius of curvature R. The top surface experiences expansion and the bottom surface experiences compression. Between these two surfaces is a neutral surface in which there is no expansion or compression due to bending.

For a substance which is thinner in one dimension than the other two such as a sheet of paper as seen in Figure 2.3, small forces can lead to large deformations. Typically, the energy required for bending is much less than the energy contained in stretching for items such as sheets of paper. A sheet of paper is very easy to bend but much more difficult to stretch and usually tears before any noticeable stretching occurs. The reason that paper is easy to bend is that very little volume change is required in bending as its thickness is small.

Analogously to the energy contained in stretching in Equation 2.5, the energy due to volume changes is:

$$E_{bend} = \frac{1}{2} Y \frac{(V - V_0)^2}{V_0} \tag{2.8}$$

where Y is the Young's modulus of the material for uniaxial extension or compression.

For a sheet with sides of equal length, L, the energy bending density is:

$$e_{bend} = \frac{E_{bend}}{L^2} \tag{2.9}$$

For a situation similar to a bilayer, one can imagine two sheets on top of one another each with half the thickness of the sheet. These sheets are assumed to be independent of one another. The energy density of one sheet with thickness $h/2$ is:

$$\begin{aligned} e_{bend} &= \frac{E_{bend}}{L^2} = \frac{1}{L^2}\int_0^L \int_0^L \int_{-h/4}^{h/4} \frac{Y}{2} \frac{((1+z/R)dxdydz - dxdydz)^2}{dxdydz} \\ &= \frac{Y}{2}\int_{-h/4}^{h/4} (\frac{z}{R})^2 dz \\ &= \frac{h^3}{192R^2} Y \end{aligned} \tag{2.10}$$

which leads to a strong cubic dependence of the bending energy density on the thickness. If the membrane is thin, then the bending energy goes down rapidly. Since there are two sheets the energy density is double that in equation 2.10, i.e.:

$$e_{bend,twosheets} = \frac{h^3}{96R^2} Y \tag{2.11}$$

Since the bending only leads to expansion and compression of the volume elements within the membrane plane, the Young's modulus Y can be expressed using the two-dimensional stretching modulus K_A.

$$K_A = Yh \tag{2.12}$$

and therefore equation 2.10 becomes:

$$e_{bend} = \frac{1}{96} K_A \left(\frac{h}{R}\right)^2 \tag{2.13}$$

Equation 2.13 shows that even substances with a high Young's modulus (like metals) can be bent fairly easily if the ratio of h/R is small. Conversely, a material with a low Young's modulus can be very difficult to deform significantly if the ratio of h/R is large.

If one wants to write the energy density proportional to the square of the deformation, then one can define another constant. Equation 2.13 can be written as:

$$e_{bend} = \frac{1}{2R^2}\kappa \tag{2.14}$$

where κ is the *bending modulus* and defined to be

$$\kappa = \frac{1}{48}K_A h^2 \tag{2.15}$$

The bending modulus and area compressibility modulus are commonly mentioned in regards to bilayer membranes. As can be seen from equation 2.15, they are proportional to one another. This equation relating the stretch and bending moduli is found in literature quite often and is sometimes used to determine the bending modulus from a known value of the area compressibility modulus K_A. However, the derivation of the above assumes a continuum approximation which may not be completely appropriate for lipid bilayers because of the complex underlying structure of lipids. Also, if one assumes that the bilayer is perfectly incompressible then there will be an additional factor of $1 - \mu^2$ in the denominator in which μ is the *Poisson ratio*. In the case of perfectly incompressible substances $\mu = 0.5$, therefore in 2.15 the factor 48 in the denominator is reduced to $48(1 - 0.5^2) = 36$. Regardless, 2.15 is a reasonable order of magnitude estimate for the bending modulus based on the stretching modulus. This relation is used to calculate the bending modulus of our bilayer from the area compressibility modulus [9]. However, experimentally the bending modulus is usually measured directly by measuring the energy required to impose some bending, or to monitor the thermal fluctuations opposed by the bending rigidity.

2.2.1 Helfrich Hamiltonian

From the previous analysis of the curved beams, the energy contained in curvature is a bending modulus multiplied by the square of a local curvature. In the case of membranes

as they are 2D surfaces they have two principal radii of curvature. In 1970, Canham proposed that the bending energy density of a isotropic (uniform in all directions) bilayer as [14]:

$$e_{bend} = \frac{1}{2}\kappa(c_1^2 + c_2^2) = \frac{1}{2}\kappa(H^2 - 2K_G) \tag{2.16}$$

where c_1 and c_2 are the principal radii of curvature. H is the mean (or extrinsic) curvature and is defined as $H = c_1 + c_2$ and K_G is the Gaussian curvature and is defined as $K_G = c_1 \times c_2$.

However in 1973, Helfrich proposed a slightly different expression for the energy density :

$$e_{bend} = \frac{1}{2}\kappa(H - c_0)^2 + \bar{\kappa}K_G \tag{2.17}$$

in which two new variables were introduced [27]. $\bar{\kappa}$ which is the saddle-splay modulus and c_0 which is the spontaneous curvature. c_0 is non-zero if there is an asymmetry between the outer and inner leaflets, e.g. if there was a difference in the lipids composing the two leaflets then there could be some intrinsic curvature associated with that difference.

The different formulations of Canham and Helfrich are the same although the Helfrich formulation includes the spontaneous curvature. Most theoretical and numerical research assumes $c_0 = 0$. (This does not apply to my vesicles as there are fewer lipids in the inner leaflet and thus it can be considered to have a spontaneous curvature.) If one integrates the energy density over an enclosed surface (such as a vesicle), the surface integral over the Gaussian curvature term will be a constant which can be ignored. If one adds an increase in energy due to in-plane stretching of the membrane, then the Helfrich equation 2.17 becomes if integrated over the surface:

$$E = \oint dS \left[\frac{1}{2}\kappa\left(H - c_0\right)^2 + \frac{1}{2}K_A\left(\frac{a - a_0}{a_0}\right)^2\right] \tag{2.18}$$

The response tension σ in the membrane due to this area expansion, $(a - a_0)/a_0$, is given

by the second derivative of the second term with respect to a

$$\sigma = K_a \alpha \tag{2.19}$$

where the stress σ is proportional to the strain α. Altogether the form in which in the Helfrich Hamiltonian is often quoted in literature is:

$$E = \frac{\kappa}{2} \oint H^2 dS + \oint \sigma dS \tag{2.20}$$

in which the free energy of vesicle has a term related to its mean curvature and another related to the tension. For numerical and theoretical studies of vesicles, the tension in the membrane is often treated as a Lagrange multiplier which enforces a constraint on the area expansion. Vesicles can only expand by small amounts before rupturing so this is a good approximation. This approximation does not apply in MD as the area expansion of the membrane is not constant and the tension in the membrane is a function of the area expansion.

For a spherical vesicle at rest with $c_0 = 0$ and radius R, and assuming the area per lipid is uniform, the free energy is:

$$E_{sphere} = 8\pi\kappa + 2\pi R^2 K_A \alpha^2 \tag{2.21}$$

The first term, the curvature energy, is independent of radius therefore the curvature energy is the same for vesicles no matter their size. However the second term, the area expansion energy, is dependent on R. For a typical GUV, if $\kappa \sim 10^{-19} J$, $R \sim 10^{-6} m$, and $\alpha \sim 10^{-2}$, then the curvature term is of order $10^{-18} J$ and the tension term is of order $10^{-16} J$ [8]. Since there is a large amount of energy associated with the stretching of the bilayer, it is often assumed that the area expansion of the membrane is minimal.

2.3 Poiseuille Flow

In my simulation a force per particle parallel to the capillary wall is applied to the fluid and to the lipids. This creates a force per unit volume which equals a pressure gradient along the length of the channel. An analogy to this is the force of gravity which can be considered to be a force per unit volume. This pressure gradient and the internal fluid friction create Poiseuille flow. This has a parabolic flow profile as will be derived below.

One can derive the equation relating pressure gradient, fluid viscosity, pipe radius, and flow rate using the Navier-Stokes equations [60]. However for a simpler derivation I will use a balance of the forces to derive the equation governing laminar flow in a pipe. If one has a cylindrical section of stream of length ΔL centred in the pipe, the shear stress acting on the outside surface is:

$$F_{shear} = \tau 2\pi r \Delta L \tag{2.22}$$

where τ is the shear stress and r is the distance from the centre line of this stream tube. Due to the symmetry of the problem, the fluid velocity should vary in the radial direction and not as a function of length or azimuthal angle. For a Newtonian fluid, the local shear stress is proportional to the strain rate through the constant of viscosity thus the shear stress τ equals $-\eta\frac{dv}{dr}$, where v is the velocity of the fluid. Therefore

$$F_{shear} = -2\pi r \Delta L \eta \frac{dv}{dr} \tag{2.23}$$

The pressure difference between the left end and the right caps of the stream tube is defined to be ΔP. Therefore the force due to this is:

$$F_P = \Delta P \pi r^2 \tag{2.24}$$

The force due to the shear stress and the force due to the pressure difference are equal in a steady-state situation and we have:

$$dv = \frac{\Delta P}{2\eta \Delta L} r dr \tag{2.25}$$

To obtain the velocity as a function of radial distance r, we must integrate using our known boundary condition. Our condition assumes the *no-slip condition* in which the velocity of the fluid is zero at the capillary wall where $r = R_P$.

$$\int_0^v dv = \frac{-\Delta P}{2\eta \Delta L} \int_{R_p}^r r dr \tag{2.26}$$

therefore:

$$v = \frac{\Delta P}{4\eta \Delta L}(R_P^2 - r^2) \tag{2.27}$$

which gives the velocity as a function of the radial distance from the centre of the tube.

2.4 Capillary Number

In order to express my results for velocity and pressure gradients in a dimensionless form, I used some key characteristics of our vesicle (bending energy modulus and radius) to define a relaxation time of the vesicle. The relaxation time of a vesicle reflects a balance of membrane elastic forces and fluid friction. For instance, when deforming a sphere by squeezing it as its poles by dr_0, the curvature energy change is approximately $\pi\kappa dr_0/r_0$ which corresponds to a force $\pi\kappa/r_0$. The fluid friction force scales with the relaxation velocity u and r_0 as $\eta u r_0 \propto \eta r_0^2/\tau$ and therefore the estimate of the relaxation time follows:

$$\tau = \frac{\eta r_0^3}{\pi\kappa} \tag{2.28}$$

This estimate overestimates the relaxation time because the deformations of a vesicle are smaller than its size [62].

The relaxation time estimate used by me and other theoretical studies ([31], [16], [20], [32]) is with the factor of π dropped. Thus characteristic time scale based on the vesicle's bending energy and radius as:

$$\tau_{shape} = \frac{\eta R_0^3}{\kappa} \tag{2.29}$$

From this, I define a characteristic velocity as [31]:

$$V_0 = \frac{R_0}{\tau_{shape}} = \frac{\kappa}{\eta R_0^2} \tag{2.30}$$

To express the velocity of the vesicle in a dimensionless format, I use this characteristic velocity and so the dimensionless velocity is defined as:

$$V* = V/V_0 \tag{2.31}$$

where V is the velocity of the vesicle. For vesicles in typical experiments, one may have $\kappa \approx 20 k_B T$, $R_0 \approx 10 \mu m$ and therefore $\tau \approx 10 s$ and $V_0 \approx 1 \mu m/s$. This would mean that a velocity of one $V*$ would be $1 \mu m/s$. In the Vitkova *et al* experiment typical velocities of their vesicles ranged from 0 to approximately 1000 $\mu m/s$ which would correspond to approximately 0 to 1000 $V*$ [58].

For our vesicle, typical values of $V*$ are from 0 to approximately 100. Our vesicle should be more fragile than vesicles in typical experiments. Our lipids have relatively short hydrophobic tails and as such should have less resistance to rupture. Experimental vesicles have long hydrophobic tails and there would be a large energy barrier to those lipids mixing in pure water.

Additionally the time scales governing bending and stretching can be compared. The time scale of stretching is:

$$\tau_{stretch} = \frac{\eta R}{K_A} \tag{2.32}$$

so the ratio of bending to stretching for our vesicle is:

$$\frac{\tau_{shape}}{\tau_{stretch}} = \frac{R_0^2 K_A}{\kappa} \approx 1000 \tag{2.33}$$

The values of R_0, κ, and K_A can be found in reference [9]; Bertrand and Joós use the same vesicle in their study of vesicle extrusion. The time scale for bending is much larger than the time scale of stretching and therefore the vesicle stretches much faster than it

bends in response to imposed stresses. This is generally true for bilayer membranes as with their fluid-like nature they do not support shear stress very well.

In my simulation, I apply a force per particle, f, which directly corresponds to a pressure gradient. The sum of the forces f on the n particles per unit volume equates to a pressure gradient $\Delta P/\Delta L$. Rather than expressing our results in terms of f, it is again helpful to find a dimensionless method of presenting the results. The most natural method is to define a dimensionless "capillary" number in which to express the flow strength like Kaoui *et al.* [33]. The capillary number Ca is defined as:

$$Ca = \frac{\tau_{shape}}{\tau_{flow}} \tag{2.34}$$

τ_{shape} is defined in equation 2.29 while τ_{flow} is the time scale of the flow. The time scale of the flow is the inverse of the shear rate, γ, which from equation 2.25 is

$$\gamma = \frac{\Delta P}{\Delta L} r 2\eta \tag{2.35}$$

For a vesicle in Poiseuille flow, I substitute the characteristic length scale, R_0, and therefore the capillary number is

$$Ca = \frac{\Delta P}{\Delta L}\frac{R_0^4}{2\kappa} \tag{2.36}$$

The values from my simulation range from 0 to approximately 20 and are comparable to the capillary numbers calculated in the studies of vesicles in Poiseuille flow [20] and [32]. For RBCs in capillaries, the average wall shear rate is around 1000/s [32]. Typical values for normal RBCs are a bending modulus $\kappa \sim 3\times10^{=19}$ [10] and a typical RBC radius (the radius of a sphere having the same area) is about $3\mu m$. The plasma viscosity $\eta \sim 10^{-3}P$. Using these values, I find a typical capillary number of ≈ 100. Kaoui et al [32] found a range of capillary numbers of 20 to 100 which reflect healthy cells. Diseased cells, such as those infected with malaria, are less deformable than healthy cells. This would result in a higher value in the bending modulus which would correspond to a smaller capillary number. Unhealthy cells can be considered to have a capillary numbers of less than 10.

2.5 Vesicles in Confined Poiseuille Flow

In this section I review current research in the field of fluid flow induced deformation of vesicles and RBCs. There are many more theoretical and/or numerical studies of vesicles in fluid flow than there are experimental papers. As such the focus is on current theoretical studies in the field. Most of the studies of vesicles in flow use the Helfrich Hamiltonian which assumes the membrane is a 2D surface with energy stored in bending and stretching.

2.5.1 Deformation of Vesicles with $\nu = 1.0$

Experimental Results

A notable experimental paper about vesicles in capillary flow was presented by Vitkova *et al.* [58]. In this paper, vesicles with a reduced volume as close to one as possible, were photographed flowing in a tube. To characterize the deformation of these vesicles, the metric of eccentricity was used. In this case, eccentricity was defined using the distance between the geometric centre and centre of mass of the vesicle and the length of the vesicle. Eccentricity was defined as:

$$e = \frac{2d}{L} \tag{2.37}$$

in which d is the distance between the geometric centre and centre-of-mass, and L is the length of the vesicle as seen in Figure 2.4. For my simulation results, I perform the same calculation and find a similar relationship between eccentricity of a vesicle and its velocity, for different confinements. As the velocity or confinement increases, the deformation increases as well. But at high velocities, the deformation of the vesicle plateaus.

I compare the Vitkova *et al.* results with my simulation results to test the validity of my model. The relationship between velocity of the vesicle and eccentricity between

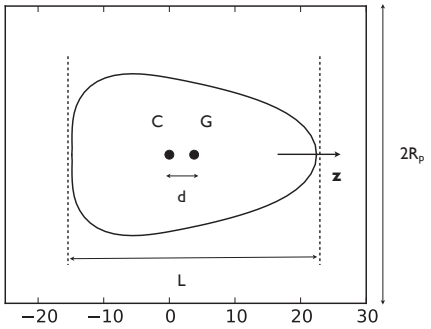

Figure 2.4: A bullet-shaped vesicle with parameters $\lambda = R_0/R_p = 0.6$ and reduced volume $\nu = 1.0$. The centre of mass is labelled with C and the geometric centre by G. Eccentricity is defined as e = 2d/L.

our sets of data is very similar. There are no error bars on the data presented in the Vitkova *et al.* paper and so it is not possible to know if my data fits within experimental error. Also the Vitkova *et al.* paper does not talk about the rupture of vesicles so it is unknown if it was possible to rupture and photograph vesicles in this situation. Finally, only shape deformation is analyzed by Vitkova *et al.* as there is no way of determining the tension from photographs. My model allows the tension profile to be determined.

Theoretical Results

In general, if one has a fully-inflated or almost fully-inflated vesicle one can calculate analytically the shape deformations using a small-deformation approximation (the assumption that the vesicle is slightly deformed sphere) [17], [20]. This approximation represents the vesicle shape as a series of spherical harmonics in powers of Δ and is only valid for vesicles with a small excess area. One of the results found is that for very small excess areas the stable shape is a bullet shape (seen in Figure 2.4) whereas a parachute-shape in Figure 2.5 is unstable. This small deformation approximation does not allow

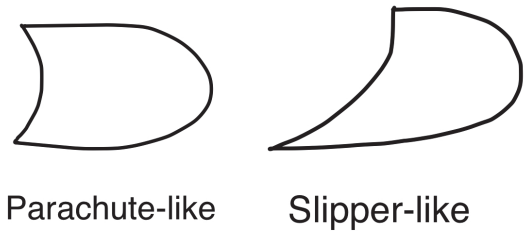

Figure 2.5: A representation of some of the various shapes that vesicles with excess area can adopt. A parachute shape is symmetric and has two tails, while a slipper shape not symmetric and has one tail.

for the calculation of large deformation and therefore the rupture of the bilayer cannot be simulated. Also this method does not allow for the calculation of the tension in the membrane. The advantage of this method is that it allows the mapping of shape as a function of capillary number and excess area.

2.5.2 Deformation of Vesicles with $\nu = 0.6$

For analyzing vesicles with a large excess area (such as in the case where $\Delta = 5$), the small deformation approximation no longer applies. In this case, numerical integration is required to solve for the shape of the vesicle membrane. One approach is the Boundary Integral Method (BIM) [56]. It is considered to be the most accurate method for calculating the deformation of large-size vesicles. It uses the well-known Helfrich Hamiltonian to calculate the membrane force at discrete points along the membrane from the local tension (a measure of stretching of the membrane) and local curvature. The fluid flow is presumed to be Stokes flow (i.e. where the inertial forces are small compared to the viscous forces) as such conditions usually prevail in the realm of cells. An iterative

procedure is applied in which the velocity field on the membrane is computed, then the position of the membrane is updated, then the force due to local tensions and curvatures is computed, then the updated velocity field is calculated, etc.. This method is often applied in 2D situations (due to computation time) [31] but can be applied to 3D as well [32].

A novel method often used to model 3D vesicles and RBCs developed by Noguchi and Gompper [45]. In this method the membrane is represented by a 3D triangular mesh; to simulate a bilayer lipid membrane, a harmonic constraint is applied to the area expansion of each triangle. Since bilayer lipid membranes have a high resistance to stretch, it is often assumed that the area expansion is small. Noguchi and Gompper also apply a global harmonic constraint on the overall volume expansion. To mimic the fluidity of the vesicle, the tethers can be flipped between two possible diagonals of two adjacent triangles. To model a RBC (which has an underlying cytoskeleton which provides extra resistance to stretching), the flipping procedure is not done. In the case where their model is modified to represent vesicles, the vesicles transit into a prolate ellipsoid shape. For their model of a RBC, the stable shape is a parachute shape.

Using BIM, Kaoui *et al.* found that vesicles can obtain both parachute- and slipper-like shapes depending on confinement and flow strength. These results do differ from the results of Noguchi *et al.* [45]. Our model of a vesicle has both similarities and some disagreement with the results of Kaoui *et al.*. This is a research area in which further studies both experimental and theoretical could be useful.

Both the slipper and parachute shapes are seen in experimental work of RBCs in capillary flow; images of RBCs' deformation through glass capillaries can be seen in the review article by Abkarian *et al.* [3]. The stable shapes obtained depend on flow strength. For slower flows, the parachute-like shape dominates and at faster velocities a slipper-like shape, seen in Figure 2.5, is common. It appears that a slipper-like shape reduces flow

resistance [32] and that vesicles start as unstable parachute shapes and then can become stable off-centre slipper shapes. This result was found in our simulations as well. Our vesicles start as parachute-like shapes but then morph into slipper-like shapes.

2.5.3 Rupture of Vesicles and RBCs

After an extensive literature searches, I found that there are no experimental papers on the rupture of a vesicle in Poiseuille flow. There are papers about the rupture of vesicles in other contexts however. Idiart *et al.* did an analytical discussion of the rupture of a vesicle due to osmotic pressure [30]. While not directly related the rupture of a vesicle in Poiseuille flow, nevertheless it does offer some insight into the pore nucleation process. When the tension in the membrane reaches a critical point, the formation of a pore becomes energetically favourable. After a pore is formed, the internal content of the vesicle begins to leak out, decreasing the tension in the membrane, leading to the eventual resealing of the pore. The same basic ideas should apply for the case of rupture in Poiseuille flow. The tension in the membrane reaches some critical level at which rupture is the likely result and the tension elsewhere in the membrane is decreased . Unlike the stationary case of osmotic pressure, however, the pore does not necessarily reseal as there is fluid flow around the vesicle.

An experimental study of the rupture of vesicles in a strong shear flow was completed in [40]. In this case, the flow field was of an arbitrary three-dimensional flow rather than a well-controlled one; the strong shear flow generated through *acoustic streaming*. While the flow profile was not Poiseuille, this paper shows images of rupturing vesicles and different breakage mechanisms. In the case where tension is a maximum one gets a sudden rupture event in which all or part of the internal liquid is ejected. The other breakage mechanism is that the tension in the membrane is nearly zero such that a tip-streaming-like process occurs, images of which are shown in [40]. In my vesicle simulations, while

the flow field is different, one can get a tensionless part of the membrane and it is from this part of the vesicle that a tether-like protrusion occurs.

The main difference between vesicles and RBCs is that RBCs have a cytoskeleton attached to the lipid bilayer membrane. This provides extra resistance against stretching and it may be that the cytoskeleton prevents extreme deformations (such as tether formation) in RBCs [36]. Images of RBCs rupturing in glass capillaries have been captured; this occurs when the RBC is tightly confined and becomes stuck in the tube. As the measured pressure builds, the RBC will burst and lose its hemoglobin and other cellular components. The remaining "ghost" RBC will continue down the tube due to the flow pressure [2], [3].

Chapter 3

Simulation Setup

Molecular dynamics (MD) is a technique which has its basis in the atomism of antiquity. Basically MD is a computational technique which solves a N-body problem of interacting spheres. The simple idea being that if you have a known number of particles which operate according to known forces, then one can solve for future states of those N particles if one knows the exact initial and boundary conditions of the problem. Newton's laws are used to integrate the future positions and velocities of the particles. However it was not until the invention of the modern computer that the first cautious simulations could be done; in the 1950s Alder and Wainwright performed such a simulation to study the interactions of hard spheres [4]. Simulations in essence become a virtual laboratory in which a system can be studied.

Of course, one has to choose the potentials, types and numbers of particles, etc. so there is a question of how well the simulation reflects reality. Therefore often simulation results are compared to known experimental results (or a known theory) in order to verify whether or not one has a plausible model. Subsequent study may lead to improvements in the model, or to its replacement, in order to explain further experiments, but this is really no different then how science is practiced in a broader context. Another thing to

note is that a model is more useful if it is not excessively complex. The minimal set of required features for the desired results is preferred if only as an application of Occam's razor and also helps determine which features are important in terms of the physical behaviour. One can always construct a more complex model through the incremental addition of features and observe any resulting change in behaviour of the system.

The setup of our system includes three main elements: the vesicle, the fluid, and the capillary; a cross-sectional view of the system can be seen in Figure 3.1. There are several types of particles, or beads, that represent the various elements of the simulation: the hydrophilic heads, the hydrophobic tails, the fluid, and the capillary. This is the same basic simulation model as was used for studying vesicle extrusion by Bertrand and Joós [9]. Which, in turn, used a lot of the same potentials between particles as defined by Goetz and Lipowsky in their MD study of coarse-grained lipids [23]. In this case, Goetz and Lipowsky used very simple coarse-grained lipids to see if they would work as reasonable models for lipid bilayers. Indeed these lipids, although not directly comparable to a particular types of real-life lipids, can self-assemble and have measurable elastic properties when they form bilayers.

3.1 The Lipids and Vesicle

My lipids consist of one head bead and two tail beads. The lipids are fully flexible which means there is no bending potential between neighbouring beads therefore there is no preferred configuration. The bonds connecting neighbouring head-tail or tail-tail beads are harmonic bond potentials defined as:

$$U_2(i, i+1) = k_2(|r_{i,i+1}| - \sigma)^2 \tag{3.1}$$

where σ is the distance between two beads i and $i+1$ and k_2 the stretching modulus is set to be $5000\epsilon\sigma^{-2}$. The stretching modulus, k_2, is set to be a large value so that the

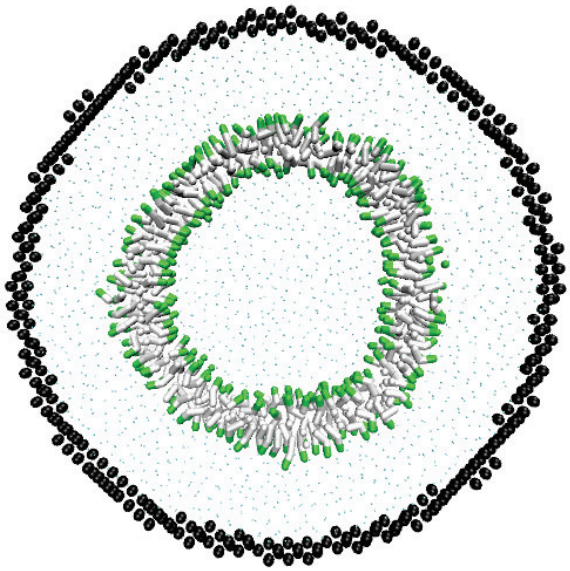

Figure 3.1: A cross-sectional view of the system where the +z direction points out of the page. The outline of the capillary (in black) is surrounds the vesicle. One can see the lipids (in green and white) composing the vesicle and thus the bilayer structure of the vesicle. The solvent is shown, but scaled down in size. In actuality the beads representing the solvent are the same size of the other particles in the system.

average length of the bonds will remain close to the value of σ [23].

A quantity known as the packing parameter describes the geometry of the lipids and is defined as:

$$P = \frac{v_t}{a_0 l_t} \tag{3.2}$$

where v_t is the volume occupied by the tail group region, l_t is the length of the hydrocarbon tail, and a_0 is the area per lipid head group. For packing parameters of less than one, the area occupied by the head group is larger than the average area occupied by the tail group and the overall geometry is of a conical shape. For a packing parameter of one, the overall geometry is cylindrical. For my lipids since the head and tail group are of the same bead size, the packing parameter is exactly one. This means that the energetically-favoured aggregate of my lipids would be a bilayer as there is no intrinsic curvature to my lipids. For packing parameters of $1/2 \leq P < 1$, the favoured aggregate geometry is that of a vesicle.

The lipids were chosen to be the simplest model of a coarse-grained lipid. This was to maximize the size of the vesicle relative to the thickness of the bilayer as there are computational limits to the number of particles that can be simulated. The vesicle was assembled such that a constant density of lipids was placed on a dividing surface between the outer and inner monolayers. The vesicle overall consists of three thousand lipids. There are more lipids on the outer leaflet than the inner leaflet. This characteristic is seen with self-assembled small unilamellar vesicles (SUVs) [41].

This vesicle is the same model as used by Bertrand et Joós. They measured the area compressibility modulus, K_A, the equilibrium area per lipid headgroup, a_0, and the half-thickness, l, of a bilayer composed of these lipids [9]. These values and others can been seen in Table 3.1. In addition the parameters that characterize the quiescent vesicle can be also be seen in Table 3.1.

Description	Symbol	Value
Equilibrium half-bilayer thickness	l_0	$2.4\ \sigma$
Equilibrium area per lipid	a_0	$1.9\ \sigma^2$
Area compressibility modulus	K_A	$8.8 \pm 0.8\ \epsilon/\sigma^2$
Bending modulus	κ	$4.24 \pm 0.36\ \epsilon$
Equilibrium area per lipid, outer heads	$a_{0,+}$	$1.85\ \sigma^2$
Equilibrium area per lipid, inner heads	$a_{0,+}$	$1.69\ \sigma^2$
Number of lipids, outer shell	n_+	1851
Number of lipids, inner shell	n_-	1149

Table 3.1: A summary of the quantities that characterize the bilayer and the vesicle. The values of l_0, a_0, and K_A were calculated from the study of a planar bilayer [9]. There is an asymmetry in the outer and inner shells due to the small size of our vesicle.

3.2 Fluid

My model has an explicit fluid (i.e., one that is modelled with particles rather than as a mean field) both external and internal to the vesicle. Other simulation work often solves for the fluid forces in the Stokes flow limit. The advantage of having an explicit fluid is that the rupture of the membrane is possible. The tradeoff is that a lot of the computational time is spent calculating the interactions of the fluid particles. The mean potential governing the interaction of the fluid is a Lennard-Jones (LJ) potential. This potential is fast to compute and includes a strong repulsive force at distances closer than the equilibrium separation and a mild attractive force at distances further than the equilibrium separation. In other words, it has both a hard-sphere repulsive force and an attractive Van der Waals force. This potential is also used to govern the interaction between other particles, such as head-fluid, tail-tail, and head-pore.

The computationally-fast (6,12) form of the LJ potential is used:

$$U_{LJ} = 4\epsilon \left[\left(\frac{\sigma}{r}\right)^{12} - \left(\frac{\sigma}{r}\right)^{6} \right] \tag{3.3}$$

where ϵ is an energy which governs the strength of the interaction and σ is a distance; this potential is the same one as used by Goetz and Lipowsky [23]. This potential defines the units of length and energy in our simulation; distances are measured in units of σ and energies in units of ϵ. The mass of each bead, whether it represents a fluid, head, or tail, is the same. By using these values to define our units for time, mass, and energy the output of values (such as velocity) in the simulation will be close to unity. Reduced, or dimensionless units, are often used to describe physical quantities from a MD simulation. A practical reason for doing this is that this reduces the risk of having values which are outside the range compatible with the computer hardware or software. But a compelling reason to use reduced units is the general notion of scaling. The idea being that a single model can describe a whole class of problems and the reduced units can be scaled to the appropriate physical units for the problem of interest.

There is a strictly repulsive potential that governs hydrophilic and hydrophobic particles thereby mimicking the hydrophobic effect. The repulsive potential, also called a *soft-sphere potential*, is defined as:

$$U_{ss}(r) = 4\epsilon \left(\frac{1.5\sigma}{r}\right)^{9} \tag{3.4}$$

For simplicity, the soft-sphere and Lennard-Jones potential have the same cutoff radius of $r = 2.5\sigma$. In order to avoid discontinuities in the potential energy and the force, the potentials are shifted slightly such that they equal exactly zero at $r = 2.5\sigma$ [23]. As there are no forces between particles greater than or equal to 2.5σ apart, this reduces the computation time.

In the simulation the vesicle is a stable structure due to the attractive LJ force between head-head and tail-tail particles and to the repulsive potential between the tail-

fluid beads. As the membrane stretches in flow, the repulsive interaction between the tail-fluid particle provides an energy barrier to pore formation. Eventually, though at high enough flow strengths the surface area expands so much that rupture becomes likely.

The capillary is composed of beads set on a face centred cubic lattice. This provides the capillary, or channel, with a degree of roughness. (The alternative would have been to model the capillary as a smooth object.) When there is fluid flow in the capillary, this creates a near no-slip boundary condition at the capillary walls. The capillary beads are connected to anchor beads (which only interact with the capillary beads) with harmonic bond of a large stretching modulus. This means the capillary is quite stiff as compared to the vesicle.

3.3 Simulation Procedure

In order to sudden stresses to the vesicle, I applied a force per particle in the simulation gradually rather than the full force at once. For a highly confined vesicle, a sudden stress causes tearing. A force (approximately 1/100th the force that can cause rupture) was applied every 10,000 time steps. This time interval was chosen such that vesicle would have time to respond before increasing the force again. At any force, this loading rate could be stopped and the force maintained in order to analyze the steady-state behaviour of the vesicle.

The tension at which a vesicle will rupture is influenced by the loading rate. At high loading rates, the tension at which a vesicle will rupture is greater, but a low loading rates the tension is lower [12]. At low rates, there is a greater amount of time for pores to develop and for ones of these to expand such that rupture is possible. By maintaining, a constant loading rate the idea is to control for this variable between different simulations.

Two open-sources software packages are used to setup the structure of the simulation and then run the simulation. The first package used is ESPresSo (Extensible Simulation

Package for Research on Soft matter) [37]; *mbtools* package from ESPResSo set the lipids onto a sphere to form the vesicle. Inside and outside the vesicle, fluid particles are placed with equal density; the solvent particles inside and outside the vesicle are labelled differently to detect rupture or leakage of the internal fluid. Once the structure of the simulation is setup and a gradual warmup exposes the system to thermal jostling, the simulation is imported in Hoomd-Blue (Highly Optimized Object-oriented Many-particle Dynamics). Hoomd-Blue is a simulation package designed for code to be run on GPUs (Graphic Processing Units) rather than CPUs or CPUs in parallel [1], [7]. With the lower cost of a GPU versus several CPUs and potentially faster computation times, GPUs are becoming an attractive choice for MD [38].

3.4 Flow Characteristics

As stated in the previous chapter, our flow profile is parabolic. It is of interest to look at the typical Reynolds number that I have when the vesicle is in motion. The Reynold's number is defined as:

$$Re = \frac{\rho V L}{\eta} \tag{3.5}$$

where ρ is the density of the fluid, V is the velocity of the object, L is a characteristic length of the system, and η is the (dynamic) viscosity of the fluid. In reduced units, typical velocities of our vesicle range from 0 to 1 $\sqrt{\epsilon\ m}$ and the characteristic length scale will be taken to be R_0 the initial radius of the vesicle. The viscosity of our Lennard-Jones fluid at the temperature of 1.0 $\epsilon\ k_B$ and density $\rho = 0.8 m\sigma^{-3}$ is 1.97 $\pm 0.16\sigma^{-2}\sqrt{m\epsilon}$ [9]. So the largest Reynold's numbers in my system are around to be a value of 7. These larger Reynold's number occur for the least confined vesicle as the velocity at the centre of the tube squares with the tube diameter.

As our Reynold's numbers are not Re $<<$ 1, our flow does not correspond to Stokes

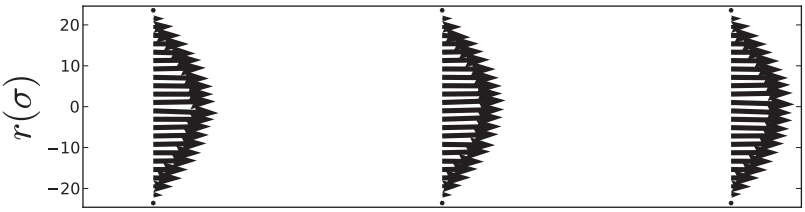

Figure 3.2: The fluid flow in the capillary without a vesicle. The length of the arrows indicates the velocity of the fluid. The capillary radius is at $r = \pm 24.6\sigma$. The velocity reaches approximately zero at the boundaries and reaches a maximum at the centre of the capillary.

flow but does correspond to the regime of laminar flow ($1 < \mathrm{Re} < 1000$). Large velocities of the Lennard Jones fluid are required to exert sufficient forces to deform the vesicle. This could be the consequence of the fact that Lennard-Jones fluid has a low viscosity and behaves more like a gas than a fluid. Lennard-Jones fluid is known to be a good model for fluids with low internal friction such as liquid argon. However, our flow profile is Poiseuille and should cause similar forces to the vesicle as in the Stoke flow limit.

A view of our flow profile without the vesicle can be seen in Figure 3.4. A parabolic flow profile develops when the force per fluid is applied in a direction parallel with the tube. The reaction time of the fluid is several orders of magnitude smaller than the reaction time of the vesicle. From chapter two, the capillary number is defined as Ca= τ_{shape}/τ_{flow} and my capillary numbers are always greater than one. While the reaction time of our vesicle, τ_{shape} is an overestimate, nevertheless I am always in the regime in which the shear rate of the flow is faster than the reaction time of the vesicle.

3.5 DPD Thermostat

A natural ensemble in which to do MD simulations is the microcanonical or NVE ensemble. In this situation, one has a thermally isolated box with volume V of N particles at energy E. However to have a system more applicable to a laboratory setup, one can also do a MD simulation using the canonical (NVT) or constant-temperature ensemble. There are various methods to apply a thermostat (or heat bath) to a MD system; all of which involve some scheme of velocity rescaling [47]. As an external force is applied in our simulation, we require a thermostat that is able to stabilize the temperature of the system, but yet still replicate momentum propagation. As we will see Dissipative Particle Dynamics (DPD) is an algorithm which can accomplish both; it employs a Langevin-type thermostat and a velocity rescaling scheme based on the local neighbourhood of a particle [28]. This preserves the centre-of-mass motion of the system.

Langevin dynamics is a tool for mathematical modelling of molecular systems in which one adds friction and noise to Newton's second law to account for unknown degrees of freedom. This works well for coarse-grained MD simulations as details are lost in using conglomerate particles and interactions are modelled as mean forces. In a system of N particles connected to a heat bath, the force on particle i is:

$$m_i\ddot{\vec{r}_i} = -\nabla U(\vec{r_i}) - \zeta_i\dot{\vec{r}_i} + F_i^R \tag{3.6}$$

where $U_r(r_i)$ is the potential energy of particle i, ζ_i is the friction coefficient of particle i, and F_i^R is the random force. The first term in equation 3.6 gives a force based on the potential energy of the particle, the second term is a friction force which is proportional to velocity, and the third term is the random force. There needs to be restrictions on the form of the random force in order to satisfy the fluctuation-dissipation theorem; a theorem which assumes that the response of a system in equilibrium to a small applied force is the same as its response to a spontaneous fluctuation. To satisfy the fluctuation-

dissipation theorem, the random force is zero on average $< \vec{R}_i(t) >= 0$ and the time correlation of $< \vec{R}_i(t) \cdot \vec{R}_i(t') >= 2k_bT\zeta_i\delta(t-t')$. This corresponds to a set of normally distributed random numbers with variance $2dk_bT\zeta_i$ and a mean of zero.

In the case of an applied external force, one can add that term $F_{i,ext}$ to the equation 3.6. However the friction term is of equation 3.6 involves the velocity of the particle with respect to the centre of mass of the entire system. Therefore in this method of velocity re-scaling, eventually the overall centre of mass motion of the system would be lost. Instead the DPD thermostat rescales the velocity of a particle with respect to its immediate neighbourhood leading to a friction term $-\zeta_i v_{i,local}$. As DPD is able to replicate momentum transport it can be an ideal thermostat to study problems involving hydrodynamics, such as the study of dynamics of complex fluids[55].

3.6 Data Analysis

Once a simulation is complete, the types of particle are outputted to a structure file and the positions and velocities to a trajectory file. The trajectory files consist of many *frames* which are snapshots of the simulation in progress. The structure files defines the types of particles in the simulation. For instance, I have several different types of particles: inner fluid, outer fluid, head, tail, and capillary. The lipid heads are classified as one type of particle in the structure file and therefore there needs to be a sorting algorithm to differentiate between which is an outer or inner head. Usually the vesicle starts as a sphere and therefore the sorting algorithm is simple. One can calculate a mean radius of the vesicle based on all the lipids head: if a head is outside this radius then it is an outer head or else it is an inner head. For each frame, the heads need to be checked if there are still an outer or an inner head as flips between the leaflets can happen (Flips are when a lipid switches from one leaflet to the other.) The algorithm for this sorting is based on a nearest neighbour type of calculation. For each lipid, if the majority of

its neighbours are outer heads then it is defined to be an outer head; conversely if the majority of its neighbours are inner heads then it is defined to be an inner head. For a real vesicle, flips are rare as there is a large energy barrier; a head would have to pass through the hydrophobic barrier presented by the tails. In the simulation, the same type of energy barrier exists and therefore such flips are a rare occurrence.

For each frame, the positions of lipid heads are triangulated; that is, a surface composed of triangles is created in which the vertices are the positions of the lipid heads. This triangulation procedure is based on Nina Amenta's Delaunay-based triangulation method called *Crust* [6]. From this surface, one can estimate the area per lipid head as one third of the average area of the adjacent triangles to the lipid [8]. This gives an area per lipid head which can be averaged over many frames.

3.6.1 Polar and Spherical Coordinates

Since the vesicle approximates a deformed symmetric ellipsoid (at least in the case where reduced volume $\nu = 1.0$), it is easiest to analyze a vesicle in 2D polar coordinates rather than cartesian coordinates as seen in Figure 3.3. (These fully-inflated vesicles are symmetric with respect to the centerline of the capillary.) The origin of our coordinate system is set as the centre of mass.

For each frame, the positions of the heads are outputted to files in order to allow for fast retrieval of the position information. One can calculate an average surface of a stable vesicle over many frames by calculating the average radial distance of the heads as a function of θ. The average surface of a vesicle can be seen in Figure 3.3 and is represented as the radial distance r away from the principal axis of the vesicle as a function of length; θ has been converted to a length in order to show the outline shape of the vesicle.

For the vesicle with reduced volume $\nu = 0.6$, it was necessary to use spherical coor-

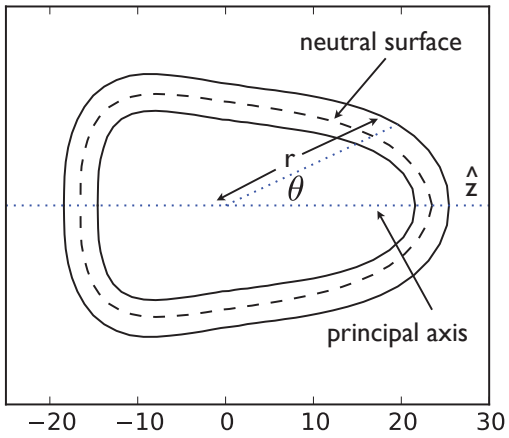

Figure 3.3: A vesicle with $\lambda = 0.8$ with the outer and inner leaflets shown as solid lines. The neutral surface, defined as the mid-distance between the outer and inner leaflets, is shown as a dotted line. In order to analyze the vesicle, I look at sections of the membrane at discrete angles of θ from $0 \leq \theta \leq \pi$. At each of these angles I look at the area expansion of the leaflets.

dinates. In order to produce a smoothed version of these vesicles averaged over many frames, it was necessary to use a coordinate system in 3D as these vesicles adopt slipper-like shapes that are not symmetric with the capillary axis. These shapes will be seen in the next chapter.

3.6.2 Triangulation

For each frame, I triangulate the head positions of the outer and inner leaflets separately. The *Crust* algorithm assumes no gaps or discontinuities on the surface [6]. An example of an triangulated surface of the vesicle can be seen in Figure 3.4. The positions of the lipids form the vertices of the surface. From the areas of the triangles surrounding a particular lipid, I can estimate the area of that lipid.

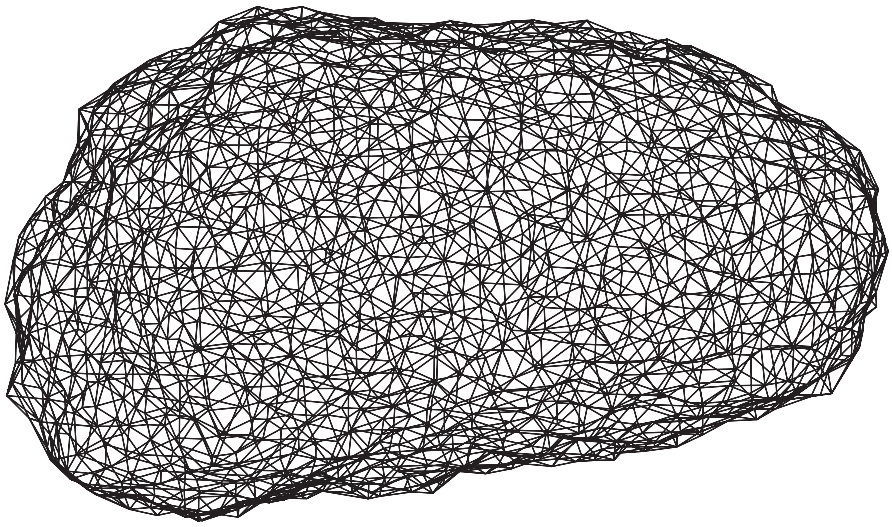

Figure 3.4: Triangulation of the vesicle surface for one frame. This shows undulations in the membrane that are not seen with the smooth surface approximation as in Figure 3.3.

The outer and inner heads were triangulated separately in each frame thus one is able to calculate a mean area per lipid head as a function of θ over many frames. This can be done for different applied pressure gradients and for different confinements as seen in Figure 4.3. This area expansion is compared to the unstressed area per lipid head of a planar bilayer $a_0 = 1.90\sigma^2$ [9].

3.6.3 Visual Molecular Dynamics

The output of a simulation can be viewed using Visual Molecular Dynamics (VMD) [29]. VMD allows the visualization of the simulation in which different particle types are coloured differently and includes many different options for customizing one's view (such as viewing subsets of particles, changing camera angle, etc) . In my case the progression of the simulation as viewed through VMD enables the visual confirmation of rupture. This is the way to know when the membrane had ruptured as can be seen in Figure 3.5.

From triangulation of the membrane (which assumption of a continuous surface), one

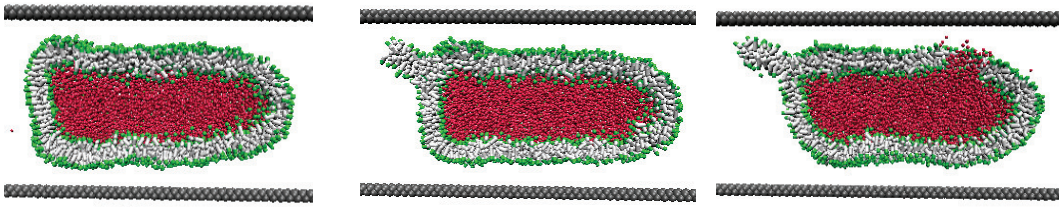

Figure 3.5: Frame shots of a $\lambda = 1.0$ vesicle as it responds to the fluid flow. In the first frame the vesicle is stable, in the second the vesicle is intact but is developing a tether-like protursion, and in the last frame the vesicle has ruptured.

can localize the point of rupture due to the large areas per lipid for the lipids surrounding the pore. If I analyze discrete sections of the membranes as a function of the polar angle θ, the bin with the largest area per lipid provides a reasonable indication of the location. The error of this location is estimated based on the size of the section.

Chapter 4

Results and Discussion

In this chapter, I look at the shape deformation of fully-inflated vesicles using both eccentricity and curvature. These results will be compared to the experimental results of Vitkova *et al.* [58]. I present the results of the triangulation of the outer and inner heads. I then use this triangulation data and the curvature calculations to calculate the area expansion of the outer heads as projected onto the mid-surface between the outer and inner heads. The idea behind this is to show the area expansion of the outer heads without the effect of bending. As this does not correlate with the eventual location of rupture, I look at the average area expansion of the outer and inner heads combined and this shows the build-up of tension in the membrane. The peak location of this average area expansion matches the rupture location. Then I calculate the fluid forces on the vesicle surface and show that the greatest contribution to the area expansion is the pressure difference between the inside and outside of the vesicle. Finally, I present the shape deformations of vesicle with reduced volume of 0.6 and compare with RBC deformation. The average area expansion is mapped onto the surface of these vesicle shapes in order to how tension varies with capillary number and confinement. A discussion of how these vesicles rupture is included as well.

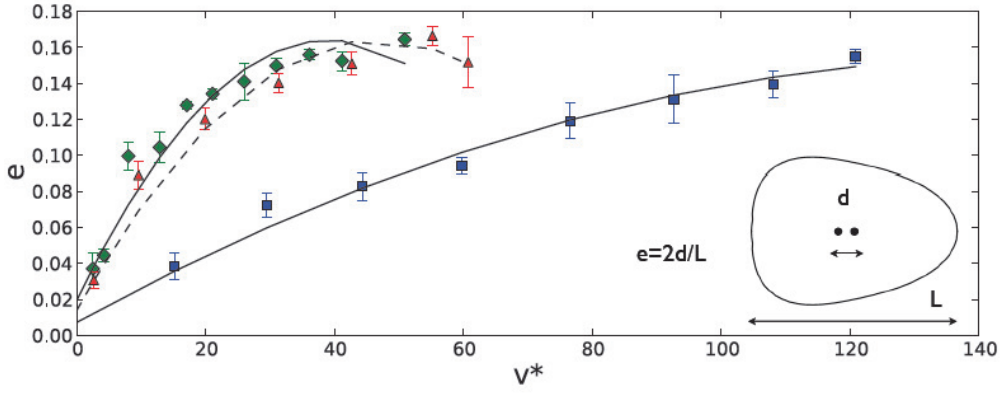

Figure 4.1: Eccentricity versus velocity for different confinements (◆) $\lambda = 0.71$, (▲) $\lambda = 0.67$, and (■) $\lambda = 0.43$. This result can be compared to reference [58]; the agreement between the two data sets is excellent.

4.1 Eccentricity

To validate the model, I first compare the deformation the model vesicle to the experimental results of Vitkova *et al.* using the metric of eccentricity. Eccentricity, e, is defined as by Vitkova *et al.*:

$$e = 2d/L \tag{4.1}$$

where d is the distance between the geometric centre and the centre of mass, and L is the length of the vesicle.

The graph of eccentricity versus velocity can be seen in Figure 4.1. Velocity is given in units of V_0 as defined in Equation 2.30; as an approximation V_0 can be viewed as being in units of $\mu m/s$ in order to compare my velocities to the velocities in the Vitkova *et al.* experiment. The velocities from the experimental data range from $[0, 1200]\mu ms$, but my velocities range from $[0, 120]\mu m/s$. This discrepancy could be due to the fact that the my vesicles have low resistance to stretching and deform at low velocities respective to their relaxation time. So while there is not a direct correspondence between my velocities and

the velocities in the Vitkova *et al.* data, my vesicles do demonstrate the entire range of deformation that the GUVs do.

The least confined vesicle can reach higher velocities with respect to the lab frame than the more confined vesicles. As the least confined vesicle occupies less of the cross-sectional area of the tube, its velocity is closer aligned with the maximum fluid velocity at the centre of the tube. The stresses imparted by the fluid flow will be less in the less confined case because vesicle should be moving at a velocity similar to the fluid surrounding it.

4.2 Curvature

Once a smoothed average surface of the vesicle is available (as seen in Figure 3.3), I can calculate the curvature along this surface. I fit a polynomial to the outline of this surface to get a function $r = f(z)$. From the symmetry of the problem there are two directions of curvature. One is tangential to the line defined by $f(r)$ and the other is the normal curvature which is perpendicular to the line. One of the principal axes of curvature is:

$$\kappa_1 = \frac{f''(z)}{(1 + f'(z)^2)^{3/2}} \tag{4.2}$$

and the second is

$$\kappa_2 = -\frac{1}{f(z)\sqrt{1 + f'(z)^2}} \tag{4.3}$$

Fitting a higher-order polynomial along the whole surface does not work at the edges due to the highly oscillatory nature of high-order polynomials at the edge of a function. This is known as Runge's Phenonmenon. Therefore I instead use a separate second-order polynomial fit along the front and rear ends to calculate the curvature. This fit is then connected to the curvature results for the mid-section of the vesicle. The different calculations of curvature result in an overall smooth function as can be seen in Figure 4.2 which presents the mean curvature as a function of vesicle length for different

confinements. As confinement increases the curvature of the front of the vesicles decreases and the stretching (as seen by the overall length represented by z in Figure 4.2) is much greater. The results presented in Figure 4.2 are consistent with the experimental work of Vitkova *et al.* [58]; the curvature at the front decreases with increasing confinement and the curvature at the back decreases with decreasing confinement.

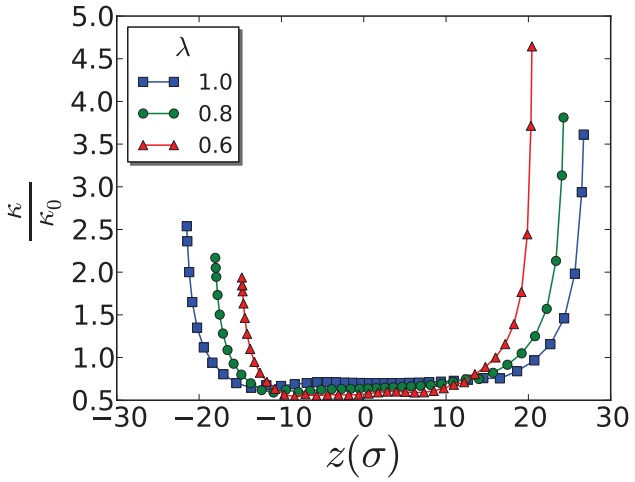

Figure 4.2: Curvature of vesicles under the same pressure gradient but different confinements. κ_0 is the initial curvature of the vesicle. The front section of the vesicles in highly curved as compared to the initial configuration and this curvature lessens with confinement. The curvature at the back decreases with decreasing confinement. The length of the vesicle is much greater in the most confined case.

This calculation of curvature assumes that the vesicle shape is well-approximated by a smooth, symmetric surface. This approximation seems to work well for the front and the sides of the vesicle, but may be inaccurate in the back of the vesicle. The back of the vesicle is under low tension (as will be seen in the next sections) and as such is prone undulations that are not seen in this smooth surface approximation.

4.3 Area Expansion of the Outer and Inner Heads

The fractional area expansion for the outer shell is α_{out} and is defined as:

$$\alpha_{out} = \frac{a_+ - a_0}{a_0} \tag{4.4}$$

where a_+ is the average area per lipid head for a particular section of membrane for the outer shell. Similarly, for the inner shell, the area expansion, α_{in} is defined as:

$$\alpha_{in} = \frac{a_- - a_0}{a_0} \tag{4.5}$$

where a_- is the average area per lipid head for a particular section of membrane for the inner shell. The average area per lipid head, $a_{+/-}$ is taken at 20 equally spaced intervals of θ.

As the pore formation is not at the tip of the vesicle, the profiles in Figure 4.3 are not very helpful in describing the rupture point. The effect of bending dominates the area expansion of the vesicle at the front tip. However, one can see a few things from these graphs. The area expansion of the outer shell is greatest for the most confined vesicle $\lambda = 1.0$ than for the two less confined vesicles for the same capillary number. (Capillary number is directly proportional to the pressure gradient and will be explained in section 4.4.) Also as the pressure gradient increases, the area expansion increases as well. The maximum pressure gradient that the vesicles are stable at is approximately the same for all three scenarios ($Ca = 20$) except for $\lambda = 0.6$ where the maximum capillary number is 17.

In all three scenarios, the area expansion of the outer shell decreases in an approximately linear fashion from the front to the rear. This is expected from the theoretical analysis of highly confined vesicles in Poiseuille flow [13]. The expansion inner shell appears to be damped as this linear decrease is not seen in the inner shell.

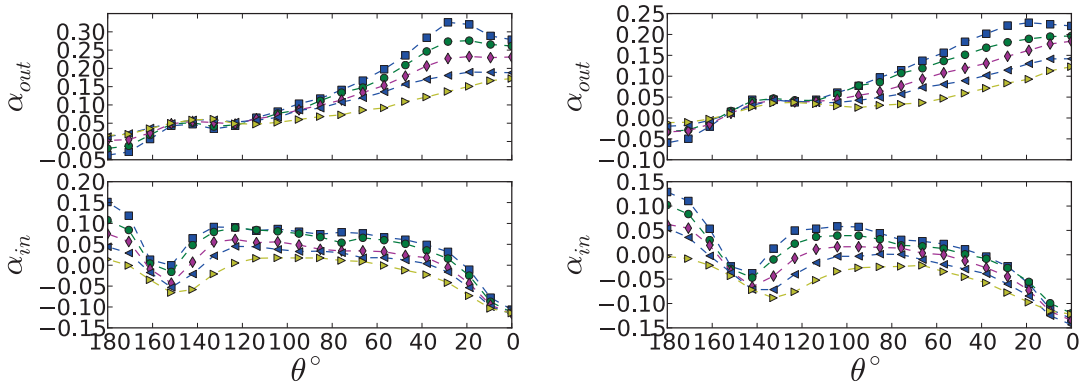

(a) $\lambda = 1.0$

(b) $\lambda = 0.8$

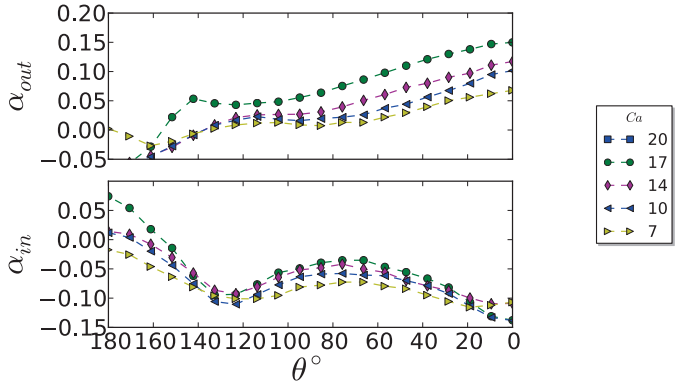

(c) $\lambda = 0.6$

Figure 4.3: The area expansion along the membrane as a function of angle θ. The greatest area expansion/compression is at $\theta = 0$ (the front tip) for most forces and confinement. This is due to the effect of bending as the membrane is highly curved at the front of the vesicle.

4.4 Area Projection of the Outer Leaflet onto the Neutral Surface

Another way to look at the response of our vesicle to external forces is to calculate the area expansion of the outer heads as *projected* onto the neutral surface. The neutral surface being defined as the mid-plane between the outer and inner shells as seen in Figure 3.3. On this surface there should be no area expansion or compression due to bending effects. If the curvature of the neutral surface and the area expansion of the outer heads are known, then one can calculate what the area per lipid head would be on this neutral surface.

If a bilayer is bent with radius R, then the outer leaflet experiences an increased area per lipid, a_{out}, and the inner leaflet experiences a compression of a_{in}. The amount of area expansion or compression is a function of the curvature (curvature as measured from the neutral surface) and the half-thickness of the bilayer, l (which is the length of the lipids). The amount of expansion is:

$$a_{out} = a_0 + a_0 lc + O(lc)^2 \tag{4.6}$$

where $c = 1/R$ is the curvature of the neutral surface and a_0 is the initial area per lipid head of the planar bilayer before bending. Similarly, the amount of compression is:

$$a_{in} = a_0 - a_0 lc - O(lc)^2 \tag{4.7}$$

Often, in theory one refers to the density of lipids so first it is of interest to convert equation 4.6 into a form based on densities, as shown below:

$$\left(\frac{1}{\rho_{out}}\right) = \left(\frac{1}{\rho_{in}}\right) + \left(\frac{lc}{\rho_{in}}\right) + O(lc)^2 \tag{4.8}$$

where ρ_{out} and ρ_{in} are the densities on the surface S_{out} and S_{in} respectively. One can manipulate the previous equation 4.8 as:

$$\frac{1}{\rho_{in}} = \frac{1}{\rho_{out}}\left[\frac{1}{1 + (lc) + O(lc)^2 + ...}\right] \approx \frac{1}{\rho_{out}}\left[1 - lc\right] \tag{4.9}$$

and the density are related to one another by a bilayer half-thickness l and the mean curvature c.

For a membrane under tension it can be convenient to base the projection calculation on a reference density that we will call ρ_{ref}. This ρ_{ref} can be different from ρ_0 the equilibrium density of a plane monolayer, as in the case of studying a monolayer under tension [11]. One can define a dimensionless density as:

$$r = \frac{\rho - \rho_{ref}}{\rho_{ref}} \tag{4.10}$$

and the relationship between the r and lc is [11]:

$$r(lc) = r + lc + O(lc)^2 \tag{4.11}$$

where $r(lc)$ is the density of lipids a distance l above the neutral surface with curvature c and r is the dimensionless density on the neutral surface. The above equation 4.11 can be rearranged into densities

$$\rho(lc) = \rho + \rho_{ref} lc \tag{4.12}$$

I can solve this for the value of ρ_{ref}. For a vesicle at equilibrium, we know the equilibrium densities ρ_+ and ρ_-, the distance between the is $2 \times l$, and the curvature of the inner surface is $c_- = 1/11.95\sigma^{-1}$ (based on the initial radius of curvature of the inner heads). Substituting $\rho(lc) = \rho_+$ and $\rho = \rho_-$ then

$$\rho_{ref} = \frac{\rho_+ - \rho_-}{2lc_-} \tag{4.13}$$

which gives a value of $\rho_{ref} = 0.127\sigma^{-2}$. This value is much less than $\rho_0 = 0.526\sigma^{-2}$ and means that the dependence on curvature is less than what would be expected for the situation in which one goes from a planar to slightly curved configuration. If I plugs back our value of ρ_{ref} into equation 4.12 and $\rho = 1.77^{-1}$ (the density of lipids on the neutral surface for a quiescent vesicle) then I find the density on the outer surface to be: $\rho_+ = 0.543\sigma^{-2}$. If this density is converted into an area per lipid, it becomes $1.85\sigma^2$ which

is the expected value for the outer shell. If $c = 0$ (the case for a planar membrane) then $\rho = \rho(lc)$ in equation 4.12 as would be expected. This calculation fulfills the expected values for these boundary conditions.

Now I want to use equation 4.12 to calculate the density of the outer heads as projected onto the neutral surface. Therefore equation 4.12 becomes

$$\rho_{proj} = \rho_{+} + \rho_{ref} lc \tag{4.14}$$

but if one keeps the second order term of (lc) then ρ_{proj} becomes:

$$\rho_{proj} = \rho_{+} + \rho_{ref} lc + 0.5(lc)^2 \rho_{ref} \tag{4.15}$$

As I present my results in terms of area expansions rather than densities, it is easy to convert ρ_{proj} into an area as:

$$a_{proj} = 1/\rho_{proj} \tag{4.16}$$

Figure 4.4 is a graph of the fractional change of the projected area of the outer leaflet $a_{proj} = 1/\rho$ with respect to a_0. Therefore $\alpha_{out,proj}$ as expressed in Figure 4.4 is defined as:

$$\alpha_{out,proj} = \frac{a_{proj} - a_0}{a_0} \tag{4.17}$$

From Figure 4.4 the back of the vesicle is under zero to negative tension. This is due to the effect of the force of the fluid pushing on the back of the vesicle. At the very tip of the vesicle ($\theta = 0$) the stress is zero and quickly rise to reach a maximum at $z \approx 30°$. The overall stress on the outer surface is greatly lessened with decreasing confinement as can been seen from subfigure (a) to (c) in Figure 4.4.

This calculation is interesting to do because it shows that the build-up of tension is close to where the vesicles will eventually rupture. It may not exactly coincide with the point of rupture because the inner leaflet could be playing a role in where the vesicles rupture. Also it is not clear if the relationship between densities as seen in equation 4.12

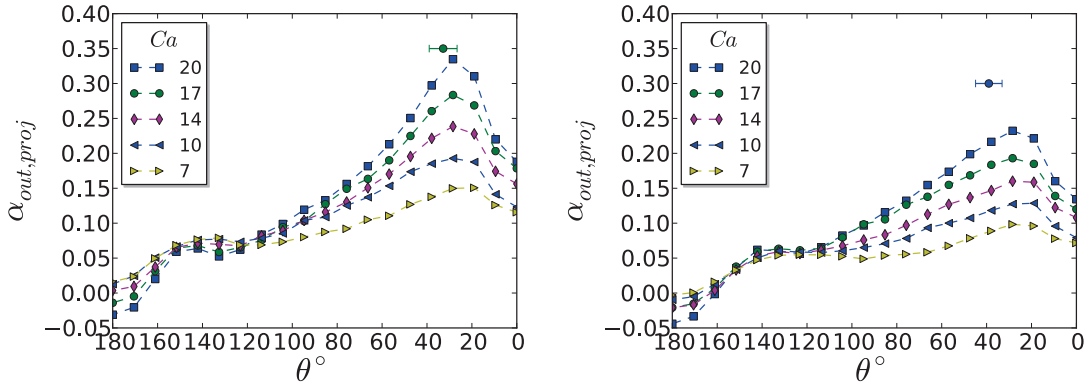

(a) $\lambda = 1.0$

(b) $\lambda = 0.8$

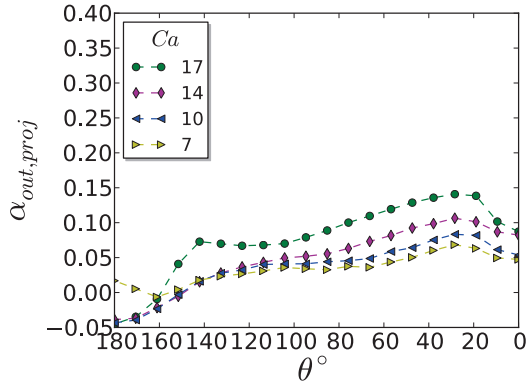

(c) $\lambda = 0.6$

Figure 4.4: The area expansion of the outer leaflet without the effect of bending as a function of θ. The angle at which the vesicle ruptures is indicated for the subfigures (a) and (b) as these highly confined vesicles will "burst" in flow. The projected area expansion shows a build-up of tension in the outer leaflet, but doesn't coincide too well with the eventual rupture point of the vesicle, as indicated by the dot with error bars.

applies particularly well to our vesicles. This equation assumes a bilayer that is slightly curved compared to some planar reference state. Our vesicle is initially curved and then the mean curvature changes as the vesicle is exposed to the flow. This could be why our calculated value of ρ_{ref} does not equal the density of lipids at the mid-surface between the outer and inner shell. Nevertheless, it will shown that is a much simpler calculation that can account for the tension build-up and eventual rupture location. However first, I will discuss the theory of pore formation in planar membranes and then some detail of how pore formation occurs in my vesicles in the next section.

4.5 Pore Formation in Planar and Curved Membranes

It costs energy to form a pore in planar membranes as the pore exposes the lipid tails to the surrounding fluid thus raising the free energy. However once a membrane is stretched to a certain point (typically strains of $\sim 4\%$ for real vesicles), the formation of a pore relieves some of the tension in the rest of the membrane and thus pore formation can become energetically favourable. The energy cost associated with the stretching of a given piece membrane is [22]:

$$E_m = \frac{1}{2} K_a a_m (\frac{\Delta a}{a_0})^2 \tag{4.18}$$

where a_m is the total relaxed area for that section of membrane, and the relaxed areal density is a_0. When a pore is inserted the area change per molecule is:

$$\frac{\Delta a}{a_0} = \frac{\Delta a_m}{a_m} - \frac{a_p}{a_m} \tag{4.19}$$

where a_p is the area of the pore and Δa_m is the expansion of the membrane. The energy of the pore is proportional to its perimeter. Therefore the energy of a stretched membrane with pore is [22]:

$$E_m(a_p) = 2\lambda\sqrt{\pi a_m}(\frac{a_p}{a_m})^{1/2} + \frac{1}{2} K_a a_m (\frac{\Delta a}{a_0})^2 \tag{4.20}$$

where λ is the edge tension (an effective edge energy per unit length). The edge tension is a constant which depends on the hydrophobicity of the tails, the length of the tails, and their rigidity.

A question becomes what happens in the case of a curved bilayer? The curvature and the thickness of the bilayer lead to different environments for the outer and inner leaflets. If both the outer and inner leaflets are stretched such that the area per lipid head is greater than the equilibrium value, then pore formation could be energetically favourable as in the planar membrane case. Conversely if both the the outer and inner leaflets are compressed with respect to a_0, then pore formation will not energetically favourable. The case in which the area per lipid as measured on the mid-plane is approximately a_0, whether or not pore formation is energetically favourable is questionable. Generally, it is found that this situation does not lead to the formation of pores in my simulations. The area as per lipid as measured at the mid-plane had to be greater than a_0 in order for rupture to occur; this is analogous to the planar case in which area expansions greater than a_0 are necessary for pore formation to be energetically favourable. Figure 4.5 provides a cartoon that illustrates pore formation, represented by the shaded boxes, in a planar and curved piece of bilayer membrane.

While the cartoon in Figure 4.5 is helpful, it is does not truly show the bending of the lipids that happens at the edges of the pore. This is the origin of the line tension in equation 4.20. As the fluid starts to infiltrate the bilayer, there is a tendency for the lipid heads to turn towards the fluid due to the hydrophobic force between the tails and the fluid. This can be seen for a top view of the rupture location in Figure 4.6.

It is also useful to view the rupture from the side as is done in the cartoon 4.5. To do so, I took a cross section of the vesicle to allow viewing of the pore. This can be seen in Figure 4.7. The rupture point is located to the upper right of the Figure. The dynamics as observed in this figure (and in other simulations) is that pore formation occurs from

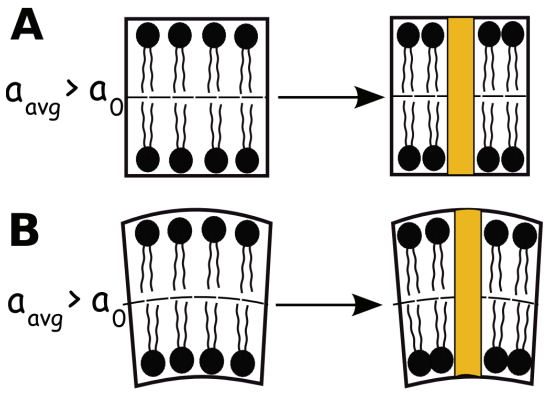

Figure 4.5: Pore formation for planar (A) and curved (B) membranes. The initial configuration in both cases is that the area per lipid, a_{avg}, as measured at the mid-surface is greater than the equilibrium value of the area per lipid head a_0. A pore, indicated by shaded box, formed in the planar case reduces the area per lipid and thereby should reduce the overall energy of the membrane. For a curved bilayer, pore formation can be favourable (as in the planar case) if the area per lipid head at the mid-surface is greater than a_0.

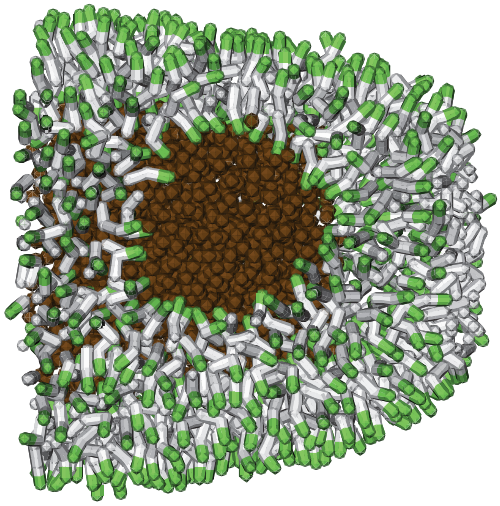

Figure 4.6: This a VMD picture taken from “above” the pore. (The word “above” is in quotation marks as there is no preferred angle of rupture with respect to the centreline of the capillary.) The lipids heads (coloured in green) are bending towards the centre of the pore. This bending increases the free energy of the bilayer. The inner fluid is shown coloured in brown.

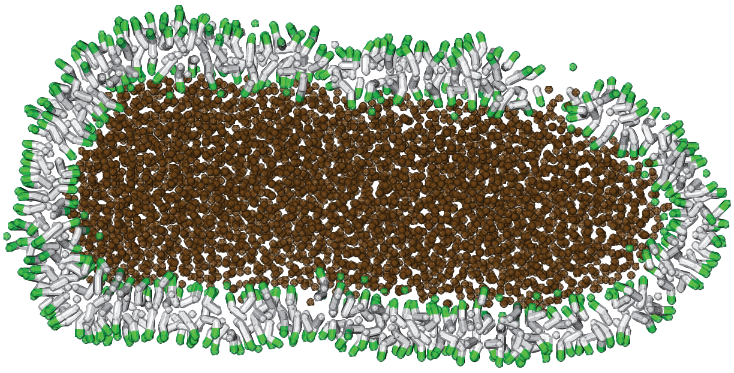

Figure 4.7: This a VMD picture taken from the "side" of the pore. As in the previous figure, the lipids are in green, the tails are in white, and the inner fluid is in brown. As the simulation progresses, this hole will become larger and more inner fluid will leak from the interior of the vesicle. The outer leaflet is more spread apart than the inner leaflet which suggests pore formation happens from the outside in.

the outer leaflet and then propagates to the inner leaflet.

4.6 Average Area Expansion

The simplest way to analyze my bilayer is to take an average area expansion of both the outer and inner heads. The vesicle surface is curved and therefore the outer heads will be stretched and inner heads will be compressed. However taking an average area expansion reduces or eliminates the effect of bending as the expansion and compression will cancel out to some extent. The main reason for taking the average area expansion is that it related to the tension. At moderate forces (which should be true for our steady-state vesicles), the average area expansion is proportional to the tension in the bilayer [18]. In Figure 4.8, the average area results are shown. The area expansion is expressed as a

fractional area expansion with respect to a_0:

$$\alpha_{eff} = \frac{a_{avg} - a_0}{a_0} \tag{4.21}$$

where a_{avg} is the average area of the outer and inner heads per lipid in a section of membrane. In essence a_{avg} represents an effective area per lipid head at the mid-surface. Figure 4.8 is the area expansion profile of the vesicle where $\theta = 0$ is the front and $\theta = 180°$ is the back of the vesicle. From Figure 4.8 one can see that α_{eff} needs to be greater than 0 for rupture to occur. The location along the length of the vesicle rupture is represented in the first two scenarios by the point at $\alpha_{eff} \approx 0.10$. For the third scenario, where the confinement $\lambda = 0.6$, the vesicle does not "burst" like the more confined vesicles as α_{eff} never rises above 0.

The area expansion profiles in Figure 4.8 are for stable vesicles; ones that have not yet ruptured nor have developed tether-like protrusions. The largest strain the membrane is capable of withstanding is around 0.10 or 10% seen in Figure 4.8 (a). This is much greater than real vesicles as the typical strains are around 4%. Fournier and Joós found that smaller vesicles can experience greater strains before rupture [22] . Larger vesicles have a larger number of potential sites from which pore formation could occur thus entropy would favour the formation of pores in larger vesicles. Another factor which influences percent strain before rupture is the flexibility of the tails. Tails with a higher rigidity are more likely to rupture at lower strains [22]. Our tails are fully flexible and this might be another factor which favours large strains in our vesicle.

The area expansion of the membrane is due to the hydrodynamic forces on the outer leaflet. The area expansions of the outer and inner leaflets of our vesicle can be viewed separately as in Figure 4.3. There is a linear decrease in area expansion in the outer leaflet from the front to the back of the vesicle (in the region excluding the front and end caps of the vesicle); this result is consistent with lubrication theory governing tightly confined vesicles [13]. This pattern was not observed in the area expansion of the inner

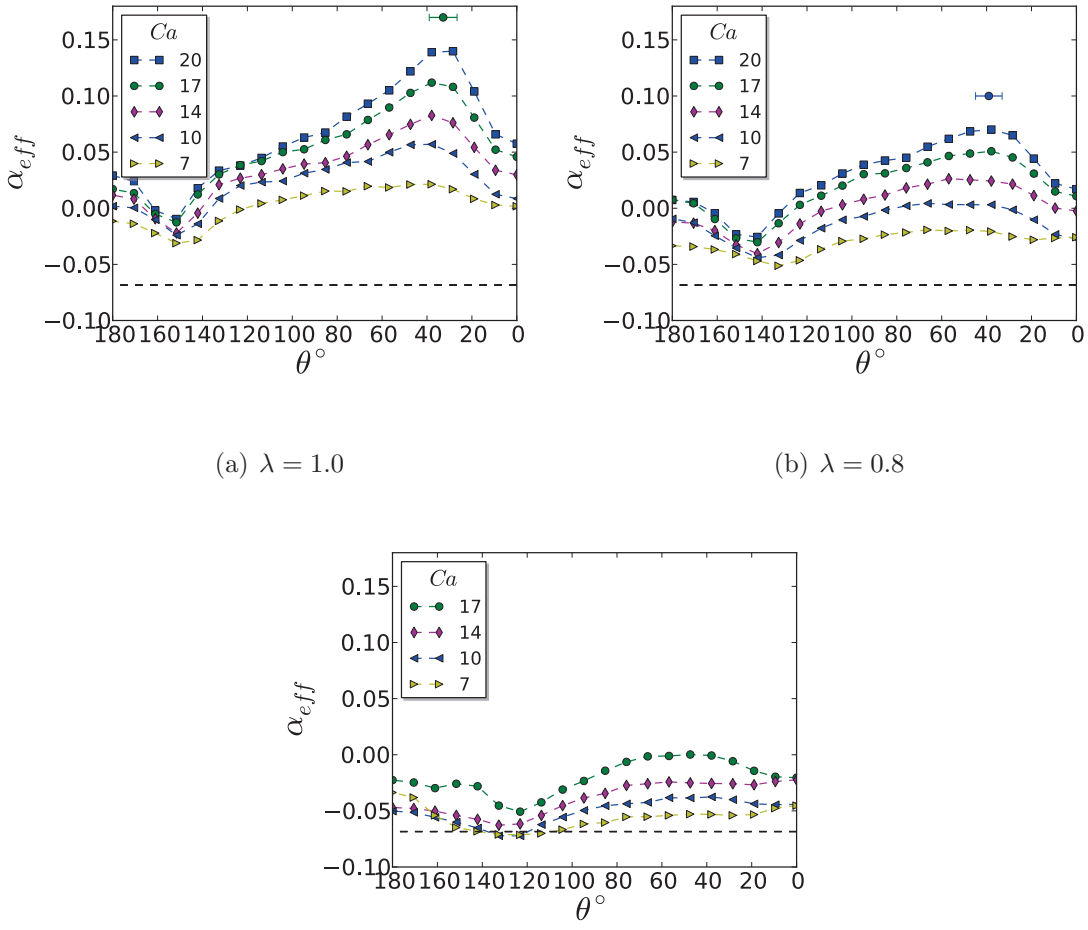

(a) $\lambda = 1.0$

(b) $\lambda = 0.8$

(c) $\lambda = 0.6$

Figure 4.8: The effective area expansion along the membrane as a function of the θ of the vesicle for different flow strengths Ca. There are clear points of rupture for the two more highly confined vesicles and occur where the effect of stretching is greatest; the point of rupture with error is labeled on the graph. For $\lambda = 0.6$ the vesicle does not stretch much in flow and as such does not rupture like the two more confined vesicles. The dotted line represents the area of the mid-plane of our vesicle as compared to a_0 for the initial configuration of the vesicle. With respect to a_0 the area per lipid on the mid-plane starts as compressed.

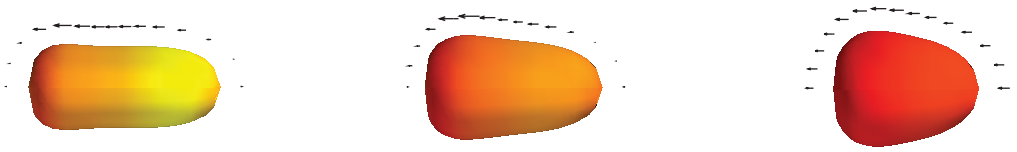

(a) $\lambda = 1.0$ (b) $\lambda = 0.8$ (c) $\lambda = 0.6$

Figure 4.9: The lighter (yellow) colour indicates the point of highest strain based on values of α_{eff} from Figure 4.8 for Ca=14. The strain is mapped onto the average surface of the vesicle to give a visual idea of the points of greatest stress. Also the fluid velocity with respect to the vesicle is shown for interest.

leaflet suggesting that the hydrodynamic forces are being dissipated through the bilayer and therefore the inner leaflet reacts very little in response to the imposed flow. The area expansion as seen in Figure 4.8 should be a combination of the applied stress on the outer leaflet and the dissipation of this force through the bilayer. In essence Figure 4.8 presents a damped view of the hydrodynamics forces applied to the outer leaflet.

One can use simple arguments to understand why membrane dissipation is significant for small vesicles. For lipid bilayers, lipid molecules are free to move within the monolayer. For typical vesicles, the two-dimensional viscosity of a lipid bilayer is about $\eta \sim 10^{-9} Ns/m$. For a typical bilayer thickness of $d \sim 5nm$, then the equivalent three-dimensional viscosity of the bilayer is about $\eta_b \sim \eta/d \sim 0.2 Ns/m^2$ [59]. This viscosity is much greater than the viscosity of water which has $\eta_w = 10^{-3} Ns/m^2$. The dissipation through the bilayer extends over the thickness d while the hydrodynamic dissipation of the surrounding fluid is over a distance of the order of the size of the vesicle R_0. Membrane dissipation is more significant if $(\eta_w/\eta_b)R_0 < d$. For typical vesicles the membrane dissipation is relevant at length scales below 1 μm, that is for small vesicles. Membrane

dissipation is significant for our vesicle due to its small size (which would not be in the case of GUVs).

The fluid flow with respect to the vesicle is shown in Figure 4.6. The fluid flow is symmetric with respect to the top and bottom of the vesicle and so is shown for the top half only. At the front of the least confined vesicle, the fluid forces is pushing into the vesicle and should reduce the tension (and thereby the area expansion) in accordance with the Young-Laplace law. Indeed the area expansion at the tip for the least confined vesicle is the smallest of the three cases in Figure 4.8.

4.7 Free Energy

Helfrich Hamiltonian describes the free energy of a bilayer:

$$e = \frac{1}{2}\kappa(c_1 + c_2 - c_0)^2 + \bar{\kappa}c_1c_2 + \frac{1}{2}K_A\alpha^2 \tag{4.22}$$

where c_0 is the initial curvature of our vesicle, $\bar{\kappa}$ is the Gaussian curvature modulus, and c_1 and c_2 are the principal radii of curvature. I do not have a measured value of the Gaussian curvature modulus, but it is reasonable to assume it is approximately the same as the bending modulus [11]. The area expansion of the membrane can be assumed to be α_{eff} as this describes the average area expansion of out lipids. From these assumptions and the measured curvatures of the vesicle, I can calculate a free energy density of the membrane as seen in Figure 4.7

The purpose of this calculation is to show that the energy contained in bending is less than the energy contained in tension. This is true for the highly confined vesicles in which the point of rupture coincides with the peak free energy density. If the bending contributed significantly to the energy density profile, then one would expect the peak free energy density to be at the front tip (i.e. the point of greatest curvature) of the vesicles. For the least confined vesicle, there is no clear pattern to the free energy profile.

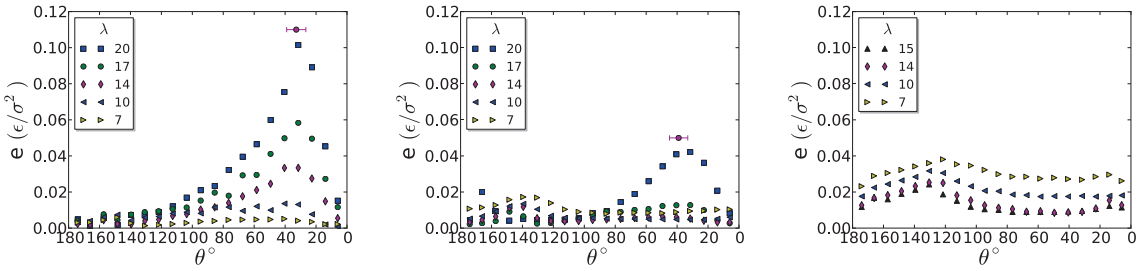

(a) $\lambda = 1.0$ (b) $\lambda = 0.8$ (c) $\lambda = 0.6$

Figure 4.10: The free energy density has calculated using the Helfrich Hamiltonian. The tension term dominates for test cases (a) and (b). There is no clear stress point for the least confined vesicle. The free energy of the least confined vesicle decreases with increasing capillary number.

Indeed it appears that the energy density decreases as capillary number increases which could be due to the overall mean curvature of the vesicle decreasing and the vesicle stretches very little in flow.

My vesicle has an intrinsic curvature c_0 because there are fewer lipids on the inner leaflet than the outer. If this was not the case, the energy in forming my vesicle would around $8\pi\kappa = 100k_bT$. This value is a couple of orders of magnitude above the thermal energy and suggests that such an object would never form naturally and if once formed, it would be unstable. The free energy density calculation in Figure 4.7 shows the change in free energy from my initial reference state. The vesicle that I construct is stable once formed. It does not rupture spontaneously in the absence of flow nor do the lipids flip between the shells readily.

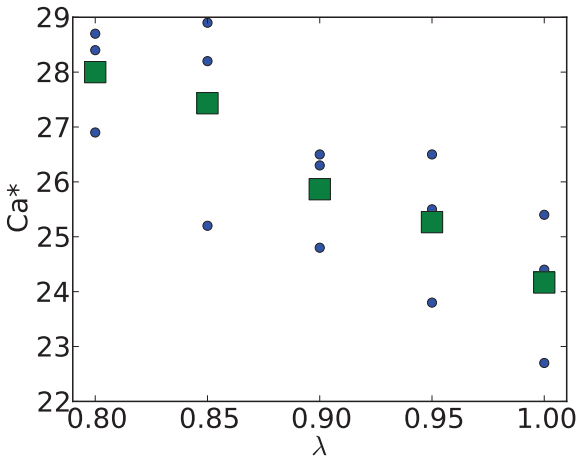

Figure 4.11: The critical capillary number, $Ca*$, at which the vesicle rupture for different confinements λ. There appears to be a linear relationship between $Ca*$ and λ for the small range of confinements studied. Confinements lower than 0.8 were not included as the vesicle breaks in flow into pieces rather than through a sudden rupture event.

4.8 Critical Capillary Number

I apply a constant loading rate (i.e. I increase the force per particle at a constant rate) until the vesicle ruptures. This critical capillary number is plotted versus confinement in Figure 4.11 for several different, independent simulations. Intuitively more confined vesicles are under greater stresses and should rupture at lower capillary numbers. Indeed this is what happens and can be seen in Figure 4.11. The capillary numbers in Figure 4.11 are higher than those in which the vesicle is stable (as represented in Figure 4.8) in which the highest capillary number is twenty. Figure 4.11 shows that the stable presented were close to their critical capillary numbers. It should be noted that the critical capillary numbers does depend on loading rate so a more complete study would have shown the effect of different loading rates on critical capillary number.

This calculation does show that if one wanted to rupture vesicles, highly confined vesicles would be the easiest to work with. These vesicles would move slower in the capillary at the same pressure gradient than less confined vesicles and would be more prone to rupture. As a real-life experiment, this could be possible to accomplish.

4.9 Forces in Membrane Displacement

Based on the Helfrich Hamiltonian, mathematically one can detail the membrane forces that cause curvature and tension changes. For simplicity, I will look at the 2D case. In 2D forces can be decomposed into normal and tangential components to the vesicle surface. The total membrane force, $\mathbf{f}$, is derived in detail by Kaoui *et al.*, and is stated below [31]:

$$\mathbf{f} = \left[\kappa\left(\frac{\partial^2 H}{\partial s^2} + \frac{H^3}{2}\right) - H\sigma)\right]\mathbf{n} + \frac{\partial \sigma}{\partial s}\mathbf{t} \tag{4.23}$$

The membrane force associated with the tension in the membrane is therefore:

$$\mathbf{f_T} = -\left[\sigma H\mathbf{n} - \frac{\partial \sigma}{\partial s}\mathbf{t}\right] \tag{4.24}$$

Tension is a force parallel to the interface [39], but is associated with a component normal to the surface (a Laplacian-like pressure component) and one associated with the change in tension along the interface.

I calculated the pressure difference, $P_{in} - P_{out}$, for the three different confinements along the contour of the vesicle and plot them in Figure 4.13. These can be used to calculate the tension according to the Young-Laplace law:

$$P_{in} - P_{out} = \sigma H \tag{4.25}$$

where H is the mean curvature and is defined as $H = \frac{1}{(R_1+R_2)}$. Using the above equation, one can calculate the expected tension due to the curvature of the vesicle and the pressure difference and the results can be seen in Figure 4.12. The fluid forces that contribute to

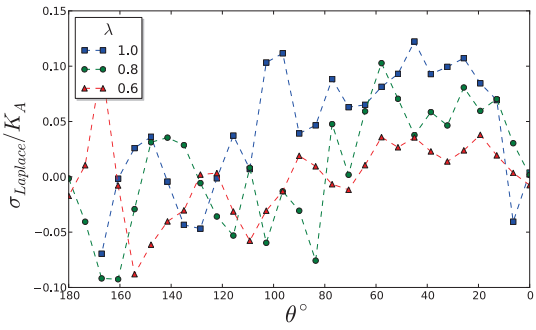

Figure 4.12: The tension in the membrane as computed by the Young-Laplace equation for Ca=14. The data is noisy due to the large variations in fluid forces, but shows a similar pattern to the average area expansion profiles in Figure 4.8.

the tension in the membrane for my vesicles are dominated by this Laplacian-like term as this tension is close, both in value and position of the peak, to the profile seen in Figure 4.8.

While the data is noisy due to the large fluctuations in the calculated forces, the data in Figure 4.12 shows that the tension at the front of the vesicles is near zero. This is due mainly to the pressure difference as can been seen in Figure 4.13. The main purpose of this is to give an idea of the major contributing forces to the displacement of the lipids. Also the fact that the pressure difference is close to zero at the back of the vesicles could contribute to tether formation as will be discussed in the next section.

4.10 Forces in Tether Formation

Vesicles are well-known for their ability to form tethers that are cylindrical protrusions from the main bulk of the vesicle. In experiments, they are formed by the application of a point force to a membrane as seen in Figure 4.14. They are also formed in less

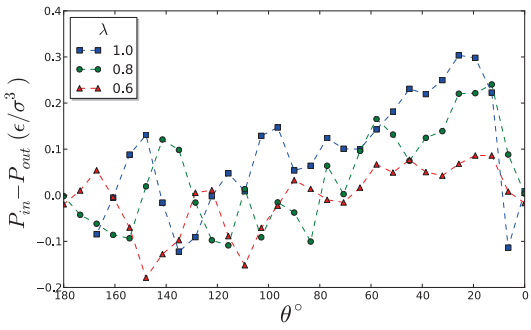

Figure 4.13: The pressure difference from the inside and outside of the membrane for different confinements for Ca=14. The pressure difference is close to zero at the rear portion of the vesicle ($\theta = 180°$) and also close to zero at the front tip.

controlled situations as well. For example staining techniques have revealed dynamic tether networks in the Golgi apparatus of living cells [50]. Also tether formation can occur if one of the monolayers is chemically modified such that the preferred area per lipid changes [21]. The resulting asymmetry in the monolayers can trigger the formation of tethers or tubules.

The radius of the resulting tether is dependent on the bending modulus of the bilayer and the tension in the membrane by:

$$r = \sqrt{\frac{\kappa}{2\sigma}} \tag{4.26}$$

This dependence on the inverse square of tension has been verified by Evans and Yeung in their classic tether-pulling experiment [19].

There is a pressure jump ΔP in the presence of a closed vesicle. However this plays little role in determining the tether radius [19]. In fact the pressure jump is approximately zero ($\Delta P \approx 0$) for tether formation [49]. Indeed this appears to the case with my vesicle as tethers form where the pressure difference is approximately zero at the back of the

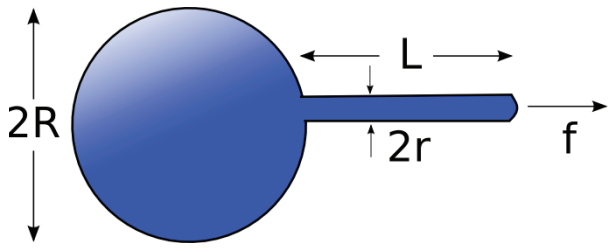

Figure 4.14: A vesicle in a tether pulling experiment. The point force f is applied to a vesicle with radius, R. The resulting tether has a radius r which is dependent on the tension and bending modulus of the membrane and the pulling force, f.

vesicles. So in the case where there is no explicit pulling force f, what could lead to tether formation in bilayers? The answer lies in the asymmetry of the monolayers. For a spherical piece of membrane, the outer leaflet is more curved than the inner leaflet. While the longitudinal tension is the same in both, the asymmetry due to bending creates a net axial force as seen in Figure 4.15. This force can lead to the formation of tethers in vesicles without an external pulling force f.

It would of interest to know if tether formation could be observed in GUVs in experiments for the particular case of vesicles flowing in a tube. It may be that since GUVs have strains of around 4% before rupture that the tether formation may be too small to be observed. My vesicles can stretch significantly before breaking and this could be contributing to this phenomenon being easily observed. It should be noted that tether formation only occurs when my vesicle is close to rupturing. Tethers are not observed in my stable vesicles.

4.11 Deformation of Vesicles with $\nu = 0.6$

For RBCs in Poiseuille flow, there are two main shapes that they adopt: the slipper and parachute shape. These shapes are very similar, but the main difference is that

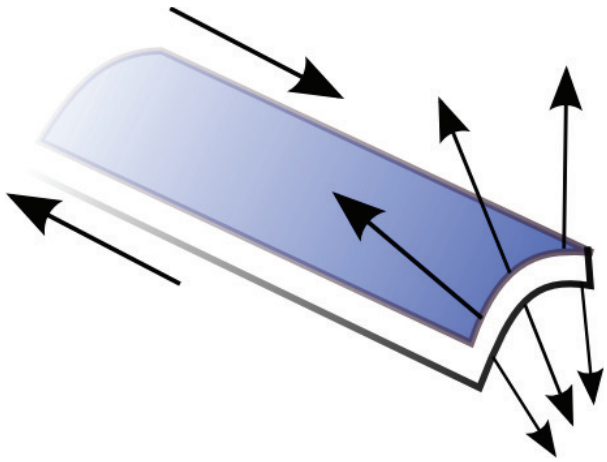

Figure 4.15: Forces on a section of curved membrane with constant isotropic tension. There is a net axial force which is equivalent to a tether pulling force as seen in Figure 4.14. The axial force can act against the tension in a membrane to create a net force which can result in tether formation.

the parachute shape is symmetric and has two tails while the slipper shape is non-axisymmetric and has one tail. The slipper shape could be considered a deformed parachute shape [54]. In my simulations, I find that my vesicles start as parachute shaped objects, but then morph into slipper-like shapes. This happens as one tail of the parachute-shaped vesicle becomes absorbed into the main body. This result has been found by Kaoui *et al.* as well [32].

The stable shapes that my vesicle assume are shown in Figure 4.16 for several different confinements and capillary numbers. These shapes can be described as slipper-like especially the shapes at high capillary numbers which have distinct tails. The capillary numbers range from zero to twenty. This is similar to the range of capillary numbers expressed by Kaoui *et al.* in their study of shape deformation of vesicles in 2D using the Boundary Integral Method (BIM). They find stable slipper-like shapes as the stable configuration for most confinements and capillary numbers except for the confinement

at $\lambda = 0.5$ where they find a parachute-shape vesicle to be stable at Ca $\approx$ 20, but I find a slipper shape. It could be that the capillary number I calculate may not exactly correspond to the capillary by Kaoui *et al.*. My capillary numbers are probably smaller for my nano-sized vesicle than with the micron-sized vesicles for the same fluid forces applied to the vesicle.

A notable result from Figure 4.16 may be the lack of any stable parachute-shaped vesicles. Generally RBCs adopt parachute shapes at lower velocities than slipper shapes as in [3], but more experimental work may be required to fully investigate the shape changes as a function of velocity and confinement. My model has no constraints on the area expansion (beyond rupturing the membrane). Also shape deformations of RBCs can be affected by the hematocrit volume fraction (the volume percentage in blood or other fluid). At high hematocrit ratio, vesicles tend to exhibit parachute-like shapes [26]. My simulation assumes a small hematocrit volume fraction of around ~ 0.01 compared to typical *in vivo* hematocrit ratios of around 0.45 in arteries and around 0.1 in capillaries.

Typical RBCs have a surface area $\sim 135\mu m^2$ and therefore have a radius of an equivalent sphere of around 0.3 μm [26]. The range of capillaries' radii range from 5 to 10 μm which results in typical confinements of $\lambda \sim 0.3$ to 0.6. As RBCs are known to adopt slipper shapes in capillaries, our slipper-like shape at $\lambda = 0.5$ would seem to be a reasonable result. Typical capillary numbers of healthy RBCs in capillaries range from around 20 to 100 [32]. Our capillary number may not be directly relatable to micron-sized objects (my capillary numbers may be smaller than for micron-sized objects), but the upper range of my capillary numbers should correspond to the fluid forces experienced by RBCs in capillaries.

As capillary number increases, the tails of my vesicles elongate. The tails of the vesicles at Ca $\geq$ 17 will eventually disconnect as the simulation time increases. Although the force applied in the simulation is slowly ramped up to avoid sudden stresses, these

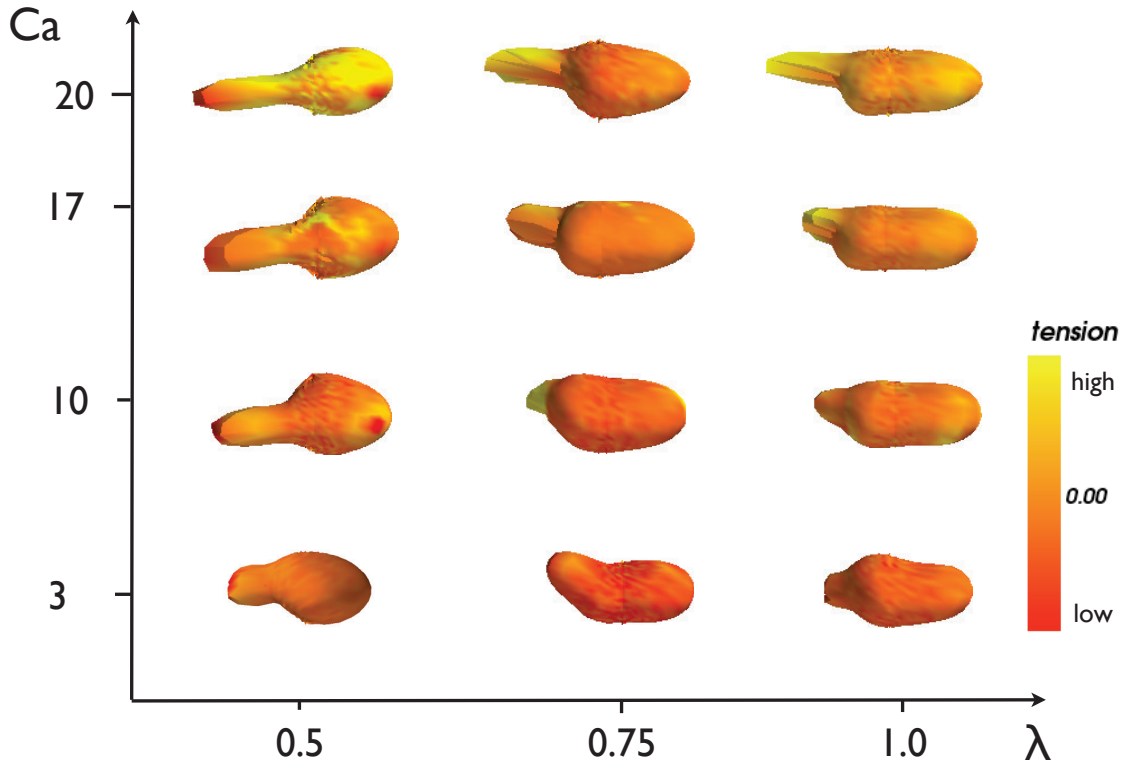

Figure 4.16: The average shape deformations of vesicles with $\nu = 0.6$ at different flow strengths and confinements. All of these shapes can be described as slipper-like. The area expansion of the lipids is mapped onto the surface. At a fractional area expansion of 0.00, the average area expansion is equal to the quiescent, tensionless vesicle. As the capillary number increases, the area expansion increase overall but especially along the tails.

vesicles are prone to leaking small amounts of inner content at the higher flow strengths as the force applied is increased. Fluid tends to leak from the back of the vesicle near where the "tail" is close to the main body of the vesicle. I mapped the area expansion onto my vesicle shapes as seen in Figure 4.16. The tails seem to experience a lot of area expansion compared to the bulk of the vesicle.

4.12 Further Discussion

Micron-sized vesicle are generally the subject of both experimental and theoretical study. These large vesicles are the subject of interest due to their size similarity to RBCs and typical vesicles used in experiments. These large vesicles are easy to describe theoretically using the Helfrich Hamiltonian. While the vesicles I study are nanometer-sized, they exhibit similar shape deformation to the larger GUVs. This happens because at the higher flow strengths, the dominating force should be the fluid not the reaction force of the bilayer. The capillary number gives an indication of the force of the fluid versus the reaction force of the bilayer and the higher numbers indicate that the fluid force dominates. Ideally the capillary number would be on the order of unity, but (as explained previously) the time scale of the relaxation of the vesicle is an overestimate. Capillary numbers can be particularly large in the case of GUVs as the time scale of the vesicle becomes an even larger overestimate. The relaxation times of the vesicle are overestimated because it is assumed to occur on a length scale similar to the size of the vesicle [62].

In the case of the rupture of the bilayer, it becomes some question of whether the rupture dynamics I observe are completely applicable to GUVs. For instance, GUVs are well-known to rupture at low strains of approximately 4% while my vesicle ruptures at area expansions around 30% of the outer leaflet. This could also be a contributing factor to tether formation in my vesicles at high flow strengths. Also the lipids that compose my bilayer are "soft" with a bending modulus of $\sim 4k_bT$. This would lead to a low

resistance to stretching as the bending modulus and area compressibility modulus are proportional to one another. This could be another factor that leads to robust tether formation as "soft" vesicles are known to exhibit tubular-connected networks in fluid flow [52]. In addition, the area per lipid asymmetry between the leaflets could also lead to tether formation as explained previously. Experimental work would be needed to discover if tether formation is significant for individual GUVs in Poiseuille flow and if it depends on the bending modulus of the lipids composing the bilayer.

The area expansion of the lipids is used as the key indicator of forces applied to the membrane. The average area per lipid from both leaflet is discovered to be the key way of describing tension in the bilayer. This method works because it is simple to apply, intuitive to understand, and successfully describes the eventual location of rupture. The location of rupture is determined by analyzing several, independent instances of rupturing vesicles. The maximal area per lipid after rupture describes the location of pore formation. I use the area expansion of the outer heads to localize the rupture point as pore formation seems to occur at the outer leaflet and then propagates to the inner shell.

Chapter 5

Conclusion

5.1 Summary of Results

In order to compare the shape deformations of my model vesicle and experimental results, I calculated the eccentricity of my vesicle as a function of velocity. The calculated eccentricities compare well with the experimental results of Vitkova *et al.*. Based on this and qualitative comparisons of shape deformations, my model of a vesicle in Poiseuille proved to be reasonable.

For a planar bilayer subjected to pure stretching (both the outer and inner leaflets stretch by the same amount) there is an easily measured area expansion. One could either measure the expansion of the outer or inner heads and would get the same measured change in area per lipid. At moderate forces this area expansion is proportional to the tension (strain) through the elastic compressibility modulus, K_A. At a critical area expansion (or equivalently a critical tension) pores are likely to form. Similarly for our vesicle a maximal local area expansion predicts the location of rupture. However, our bilayer is not planar but curved and it becomes a question of where to measure the area expansion to best predict the location of rupture. From our triangulation of the outer

and inner heads positions, we can easily detect maximum area expansions of the outer and inner head separately. For the outer heads, the greatest local area expansion is at the tip. This is not surprising considering the small scale of our vesicles and therefore the effect of bending at the front tip causes large area expansions (as measured by the outer heads). This can be seen in the corresponding strong compression of the inner heads at the tip. If one looks at the curvature of the vesicles as a function of length, then one can see quite clearly that the vesicles are highly curved at the front. As the point of rupture is not at the tip of the vesicle, the area expansion of the outer heads (based on triangulation) does not provide a good prediction of the rupture point.

The average of the outer and inner local area expansions provides the best explanation for the location of rupture. Averaging the area expansion of the outer and inner heads, a_{avg}, is in effect giving the local area expansion of the neutral surface. An approach of *projecting* the outer leaflet area expansion onto the neutral surface between was attempted to see if the location of rupture coincided with the outer leaflet expansion minus the effects of bending. However the maximum of a_{avg} (or equivalently α_{eff}) coincided better with the eventual location of rupture. This suggests that the inner leaflet plays a role in where vesicles rupture.

I studied vesicles with three different confinements: $\lambda = 0.6$, 0.8, and 1.0. The area expansion profile is greatly impacted by confinement. Highly confined vesicles ($\lambda \geq 0.8$) show significantly larger area expansions than the less confined vesicles. This large area expansion led to the rupture of these vesicles. For the least confined vesicle $\lambda = 0.6$, the area expansion is less and as a result this vesicle formed tethers rather than bursting in flow.

I expressed the applied pressure gradient in the form a dimensionless capillary number. The capillary number is defined based on the vesicle's nominal radius, the bending modulus, and the pressure gradient. This exact form was used in several other papers.

The idea is to have a dimensionless expression of my results such that they could be more easily understood and potentially used by other research groups. Unfortunately, my capillary numbers are not directly relatable to the values expressed in other works. My capillary numbers range from 0 to 20. However, capillary number can span several decades [16]. This is due to the fact that the calculation of the capillary number yields an overestimate and this overestimation increases with the nominal radius of the vesicle. It would be better to more accurately describe the relaxation time of the vesicle in order to have capillary numbers on the order of unity. This would perhaps allow for the results presented in this thesis to be more applicable to other experimental and theoretical studies.

For vesicles with reduced volume $\nu = 0.6$, I sampled the shape deformation for different capillary numbers and confinements. This result is most easily compared with the results from Kaoui *et al.* who performed a similar experiment using BIM in 2D [32]. There is some agreement between the results, but my vesicles do not show parachute-shaped vesicles at $\lambda = 0.5$ for moderate flow strengths ($\mathrm{Ca} \gtrapprox 17$). This could have been a function of the large area expansions possible in the membrane (area expansions are assumed to be small in the study by Kaoui *et al.*) or could be a consequence of the properties of the capillary. It is not possible to increase the flow strengths further to see if that would result in steady-state parachute-shapes as the membrane cannot withstand such forces without breaking.

5.2 Summary of Contributions

My Molecular Dynamics simulation of the deformation and rupture of vesicles with coarse-grained lipids in Poiseuille flow achieves two main goals. First, it provides another method to simulate vesicle deformation and, in particular, to allow for quantitative analysis of the area expansion of the lipids. The overall deformations of my vesicles are very

similar both quantitatively and qualitatively to micron-sized vesicles. It may be that methods such as BIM could allow for the expression of the area expansion of the lipids, but this has not been found in the literature to date. The area expansion is related to the tension in the bilayer which is related to rupture at strong flow fields.

The shape deformation and area expansion of vesicles with reduced volume, $\nu = 0.6$, is calculated for several different confinements and capillary numbers in Figure 4.16. This is unique in that the area expansion of vesicles has not been mapped onto the vesicles shapes. The area expansion increases with pressure gradient and the "tails" of the slipper-like vesicles tend to have high area expansions.

The second achievement of this model is that it is possible to rupture the vesicles. This is novel as this phenomenon has not been studied theoretically. Indeed as most other models assume an impenetrable surface (for ease of calculating the dynamics) it was not previously possible to study the rupture of vesicles in a fluid flow, theoretically or numerically. Also most theoretical methods assume small local area expansions of the membrane which would prevent the calculation of unstable behaviour of the membrane such as buckling or tether formation. The rupture of fully-inflated vesicles in Poiseuille flow has not been studied experimentally and so hopefully our model could inspire experimental work in this area.

However, the rupture of my "floppy" vesicles may not be applicable to RBCs that have a cytoskeleton. My vesicles stretch until they break into pieces in the flow, but RBCs have a cytoskeleton that would presumably prevent such large area expansions. Also the cytoskeleton is not fluid like a bilayer and the way a cytoskeleton would break could differ from the bilayer. Nevertheless, there are no numerical studies on the rupture of vesicles in Poiseuille and very little experimental data of RBCs rupturing. This study is novel and could inspire further work in this area.

The rupture of fully-inflated vesicles could be of interest to experimentalists who

design or fabricate liposomes for drug delivery. For instance, the rupture of vesicle in confined environments could be applicable *in vivo* as in the case of ischemia (the constriction of a blood vessel causing restriction in blood flow). Also the rupture of fully-inflated vesicles in confined tubes could be used to limit the size of vesicles in applications such as liposome fabrication.

5.3 Future Work and Open Issues

One of the current issues is the size limitations imposed by modelling every particle that composes the vesicle, fluid, and capillary. One way to enlarge the size of the vesicles would be to replace the fluid and capillary by modelling the fluid field forces by assuming Stokes flow and solving for the Navier-Stokes equations. This would retain the fluidity of the bilayer model but reduce the computation time associated with modelling the external and internal fluid. Also one would be able to have larger capillaries as there would be fewer fluid particles to calculate. When a vesicle is not highly confined ($\lambda \leq 0.4$), it is possible for vesicles to adopt a stable, off-centre position in the capillary. The membrane exhibits "tumbling" behaviour in which the bilayer rotates due to the difference in fluid forces at the top and bottom of the vesicle.

Another way to enhance my model of this vesicle would be to use more "realistic" coarse-grained lipids. There is a method of systematically coarse-graining lipids called the MARTINI Force Field [42]. In this case, one could pick a particular type of lipid, such as Dipalmitoylphosphatidylcholine (a commonly known lipid) to compose the bilayer. This would increase the number and types of particles required to form a lipid. There would be more types of forces to calculate as the lipids contain more complex sub-groups such as phosphate groups, etc.. Altogether this would increase computation time, but would provide a more realistic model for the fluid and vesicle. This should allow for a better conversion of the natural MD units of the simulation into SI units.

As with any MD simulation, it is possible to vary the parameters fairly easily. The properties of the capillary could be modified to examine the effect of a “saw-tooth” capillary. Perhaps more interesting choice may be to construct a primitive cytoskeleton attached to the inside the vesicle to model a RBC.

Currently, my research group is exploring the rupture of this vesicle model in the context of Atomic Force Microscopy (AFM). To simulate the ”poking” of an AFM cantilever, we are squeezing a vesicle between two plates. With the computational power of GPUs it should be possible to simulate more and more realistic biological objects, such as vesicles and RBCs, in any imaginable scenario in the future.

Appendix A

Appendix: *Deformation and Rupture of Vesicles in Confined Poiseuille Flow*

Deformation and Rupture of Vesicles in Confined Poiseuille Flow

Alison Harman, Martin Bertrand, and Béla Joós
Ottawa-Carleton Institute for Physics
University of Ottawa Campus
Ottawa, Ontario, Canada, K1N 6N5
(Dated: August 27, 2013)

Abstract

Vesicles are defined by a few key characteristics (such as size, reduced volume and bending modulus), but display complex, non-linear dynamics in fluid flow. We investigate the deformation of vesicles, both fully inflated and those with excess area, as they travel in tightly confined capillaries. By varying both channel size and flow strength, one is able to view vesicles as they transition from steady-state to unstable shapes, and then rupture in strong flow fields. By employing a particle-based, coarse-grained molecular dynamics model of the vesicle, fluid, and capillary system, one is able to rupture the bilayer. This is unique in that most theoretical methods model the membrane as a continuous surface. Highly confined, fully inflated vesicles show the greatest stress and rupture near their front tip. Deformation of vesicles with reduced volume, $\nu = 0.6$, is similar to other studies.

I. INTRODUCTION

Studies of the rheological properties of lipid bilayer vesicles and cells such as erythrocytes, or red blood cells (RBCs), in narrow channels are motivated first and foremost by the importance of the latter in nutrient transport within the vasculature and the use of the former as drug carriers [**check further refs**] [1]. These soft deformable objects are also being manipulated in micro- and nano-fluidics devices for research purposes and in the development of point-of-care solutions. Multiple experimental [2] and theoretical/computational studies [3–10] have been conducted on the topic. However, few, if any, address the issue of rupture due to stresses induced by hydrodynamic interactions with the surrounding fluid. Consider, for example, small unilamellar vesicles (SUVs) dubbed liposomes that are to be prepared and loaded with a potent molecular agent to be delivered to a specific site. It would be highly useful to know if, when, and where rupture and content leakage occur.

Very few experimental studies can be found on the pressure induced transport of vesicles in narrow channels. To the best of our knowledge, Vitkova *et al.* [2] are the only ones who have tackled the issue in a quantitive manner as they measured shape deformation as a function of vesicle velocity for a variety of parameters.

A lipid bilayer has little resistance to bending and as such the boundary of the membrane is highly fluid. It has been a long-standing problem in science and engineering to solve for the boundary of the membrane while immersed in an external fluid field. An experimental work dealing with fully-inflated vesicles is the research done by Vitkova *et al.* in which the shape deformation of vesicles as a function of vesicle velocity was studied quantitatively [2]. Other experimental studies have been done on bubbles and capsules. Much theoretical work has been devoted to the calculation of membrane deformation and behavior under confined fluid flow. In the case of fully inflated vesicles shape can be analytically solved assuming small deformations from a sphere [9].

For vesicles with excess area, various techniques have been applied. There is the computationally-intensive Boundary Integral Method (BIM) which solves for the position of the membrane at discrete points assuming Stokes flow conditions. The reaction of the membrane is modelled using the Helfrich Hamiltonian [11] in which the energy of the membrane is held in curvature and in tension (elastic-stretching). This technique has been applied by Kaoui *et al.* in two dimensions [4] and recently in three dimensions [6]. As the membrane has a large resistance to stretching and little to bending, it is assumed that the area expansion of the membrane is limited. Using this property, another class of models are mesh models in which a surface is defined by triangles in which the local area and global volume expansion of the mesh are constrained [8], [3]. Our technique for modelling vesicles, both fully inflated and those with excess area the same as RBCs, uses a coarse-grained molecular dynamics simulation in which the lipids (composing the membrane) are all explicitly modelled. There are no constraints on area and the volume expansions of this membrane and as such it is possible to model both unstable vesicles and their subsequent pore formation and rupture.

Our CGMD studies show vesicle behaviour and shape deformations in agreement with earlier theoretical [6] and experimental [2] studies. A new feature of our work has been the mapping of the tension along the surface of the vesicle under flow. The location of maximum tension predicts the point of rupture at large pressure gradients. We vary both the size of the channel and the pressure gradient. For vesicles which are highly confined, they tend to "burst" and lose all their interior contents. The rupture of vesicles has been studied in various contexts such as osmotic pressure [12] and other conditions of high bilayer tension such as through micropipette suction [13], [14]. However our study of vesicles in the context of Poiseuille

flow is novel. This research could be applied to the design of liposomes or applied in microfluidics in which individual particles, such as vesicles, can be manipulated under controlled conditions.

In this paper, in summary, we vary the size of the capillary with respect to a constant vesicle size and analyze the effect of confinement, flow rate, and excess area on the deformation and rupture of vesicles. The results section IV is organized as follows. First, we compare the deformation of fully-inflated vesicles with experimental data and find good agreement. Second, we calculate the tension profile of fully-inflated vesicles which are axisymmetric and find a peak stress point near the front tip. This peak stress point coincides with the eventual point of rupture for these vesicles. Third, we calculate the shape deformation of vesicles with excess area of five (the same excess area as RBCs) and compare our results to other theoretical studies on vesicles and experimental studies on RBCs.

II. THEORY

We apply a force per particle in the simulation to the fluid and lipid particles; this is the physical equivalent of, say, the force of gravity in which the gravitational force applies to each individual atom. The result of this force and the friction due to the fluid and lipids results in a steady-state situation in which there is an effective pressure gradient along the length of the channel, and the fluid and vesicle move at a constant velocity along the channel. In essence, Poiseuille flow is recreated.

In order to have a dimensionless format in which to express the applied pressure gradient and the resulting velocities, we look at defining characteristics of our system. We have a known bending modulus, κ, of our bilayer, an initial radius of our vesicle R_0, the viscosity of the external fluid η, and the area compressibility modulus K_A [15]. The values of these constants can be found in the next section which describes the simulation model. The units are based on the Lennard-Jones (LJ) force between like particles, the mass of the particles and the constant temperature of the system. From these constants one can look at the time-scales which define the system. There is a time-scale associated with bending [4]:

$$\tau_{bend} = \frac{R_0^3 \eta}{\kappa} \tag{2.1}$$

and a time-scale associated with stretching

$$\tau_{stretch} = \frac{\eta R_0}{K_A} \tag{2.2}$$

and a time-scale associated with the shear rate of Poiseuille flow

$$\tau_{flow} = \left(\frac{\Delta P}{\Delta L}\frac{R_0}{2\eta}\right)^{-1} \tag{2.3}$$

Substituting our values for R_0, K_A, κ, and η, we find that $\tau_{bend} \sim 2600ts$ and $\tau_{stretch} \sim 5ts$ where ts stands for a time step. This means that the vesicle can stretch very quickly in flow before it can adopt a shape change. In general this is true for vesicles as bilayers are very fluid and offers little resistance against shear forces. The ratio of τ_{bend} to $\tau_{stretch}$ is

$$\frac{\tau_{bend}}{\tau_{stretch}} = \frac{R_0^2 K_A}{\kappa} \approx 1000 \tag{2.4}$$

in which the viscosity of the external fluid cancels. If we substitute a typical value for a pressure gradient, $\Delta P/\Delta L \sim 0.01\epsilon/\sigma^4$, we find that $\tau_{flow} \sim 30ts$. (ϵ is our unit of energy and σ is our unit of length.) Our observations are taken every 5000 time steps and therefore our vesicles are steady-state objects at the time of observation for moderate forces. At high forces, vesicles become unstable such that rapid stretching of the outer leaflet occurs.

From these characteristic times, one can define a dimensionless capillary number, Ca, which is proportional to the shear rate (a controlled variable):

$$Ca = \dot{\gamma}\tau_{bend} = \left(\frac{\Delta P}{\Delta L}\right)\frac{R_0^4}{2\kappa} \tag{2.5}$$

where $\dot{\gamma}$ is the shear rate of the flow and equals the inverse of τ_{flow}. The capillary number is independent of the viscosity of the fluid. The capillary number defined in equation 2.5 has been employed in several theoretical and experimental works used to describe vesicle shape deformations [6], [16], [9]. Capillary numbers give an indication of the effect of bending of the membrane as compared to the shear stresses imparted to the membrane. For low capillary numbers the two factors are comparable, and at high capillary numbers shear stresses dominate and determine the vesicle shape.

However this dimensionless capillary number is not independent of vesicle size. For the same pressure gradient one can have capillary numbers which are larger due to the dependence of Ca to the fourth power of vesicle size. While larger vesicles are more fragile and break at lower pressure gradients than small vesicles, the range of capillary numbers is still greater with larger-sized vesicles. This is true with our model. If one increases the size of the vesicle, then it can reach higher capillary numbers before breaking even though the larger vesicle breaks at a lower pressure gradient. Coupier *et al.* studied vesicles with small excess areas using a numerical method over several decades of capillary number; it was found that vesicle shapes depended strongly on confinement and reduced volume much more than capillary number for confinements greater than $\lambda \geq 0.5$ [16]. We study fully-inflated vesicles with $\lambda \gtrapprox 0.5$ and achieve a similar shape deformation as GUVs in capillary flow as will be seen in our results section.

To look at the effect that the imposed fluid flow has on the vesicle, we triangulate the positions of the outer and

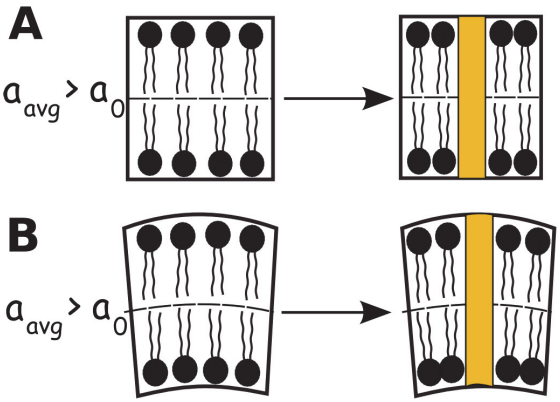

FIG. 1. Pore formation in planar (A) and curved (B) membranes. Here the area per lipid head a_{avg} (which is the average area per lipid head of the outer and inner heads) is greater than a_0 (the area per lipid head in a tensionless planar membrane) before pore formation. If a_{avg} is greater than a_0, then it is possible for pore formation to occur as indicated by the shaded box to occur.

inner lipids heads using the *Crust* surface reconstruction algorithm [17]. From the known positions of the lipid heads, the Crust algorithm constructs a surface of triangles and the basis of the vertices are the lipid head positions. This algorithm assumes a continuous surface. From these triangles, one is able to calculate an area per lipid head, a. The strain in the bilayer is measured by the fractional area expansion $\alpha = (a - a_0)/a_0$ where a_0 is the equilibrium (unstressed) area per lipid. At moderate forces, the strain, α, is linearly proportional to the stress or tension, γ through the area compressibility constant K_A, i.e. $\gamma = K_A\alpha$. At a critical area expansion (or, equivalently, a critical tension) the bilayer is prone to form pores. Our vesicle is curved and in order to extract this critical area expansion, we average the area expansion and compression of the outer and inner heads respectively in order to find the average area per lipid in a section of membrane. In Figure 1, a_{avg} equals $(a_+ + a_-)/2$ where $a_{+/-}$ is the average area per lipid for the outer (+) or inner (+) monolayers.

For a curved, unstretched section of membrane the expansion of the outer heads should equal the compression of the inner heads. By averaging the area expansion of the outer and inner heads, we extract an effective area expansion as would be measured on the mid-plane of the bilayer. If the bilayer undergoes stretching, then that area expansion due to stretching will be reflected in the value of a_{avg}.

III. THE SIMULATION MODEL

The parameters governing our molecular dynamics model are the same as were used in Bertrand and Joós paper which studied vesicle extrusion through a pore [15]. Rather than studying extrusion, this paper will be analyzing shape deformations in capillary flow and, in particular, how vesicles rupture. A brief outline of the model will be provided in this section, but further details can be found in reference [15].

TABLE I. The vesicle at equilibrium

	Outer (+)	Inner (-)
radius	16.5 σ	11.5 σ
area per lipid	1.86 σ^2	1.68 σ^2

The model is a CGMD simulation with an explicit solvent. The interactions are modelled using Goetz and Lipowsky's set of potentials [18] in which they simulated coarse-grained lipid bilayers in a L-J fluid. These potentials form the basis of the units in the system in which σ is the unit of length, m of mass, τ of energy, and ϵ of energy.

Our lipids consists of three particles, one of which represents the hydrophilic head and two of which represent the hydrophobic tail. To characterize a bilayer made of these lipids, we simulated a flat bilayer made of these short lipids and immersed in the LJ solvent. It was found that the unstressed area per lipid head was $a_0 \cong 1.9\sigma^2$, the equilibrium bilayer thickness $l \cong 4.8\sigma$, and the area compression modulus $K_A = 8.84 \pm 0.76\epsilon/\sigma^2$ [15]. The bending modulus was calculated to be $\kappa = K_A l^2/48 = 4.24 \pm 0.36\epsilon$. The vesicle and fluid are kept at a temperature of $1.0\epsilon = k_bT$ therefore our bending modulus in units of k_bT is $\approx 4.2k_bT$. Our bilayers are "soft" as the bending modulus is the same order of magnitude as the thermal energy.

A vesicle which is composed of 3000 lipids was found at equilibrium to have a outer radius of $R_0 = 16.5\sigma$ and an inner radius of $R_- = 11.5\sigma$. The outer and inner leaflets (referred to with the + and − symbols respectively) have different equilibrium areas per lipid head with $a_{0,+} = 1.86\sigma^2$ and $a_{0,-} = 1.68\sigma^2$. $a_{0,+}$ is close to the unstressed area per lipid head of a bilayer. The inner layer is more compressed than the outer layer, but this is characteristic of self-assembled small unilamellar vesicles [19]. A summary of these values can be seen in Table I.

The thickness of the bilayer membrane is of the same order of magnitude as the equilibrium radius R_0. Considering that an estimate of the thickness of a bilayer is $\sim 5nm$ and that the thickness of our membrane is $\sim 5\sigma$, then the radius of our vesicle is $\sim 16nm$. (A more detailed analysis of our the units σ, m, and ϵ as converted in SI can be seen in reference [15].)

IV. RESULTS

A. Deformation of vesicles with $\nu = 1.0$

In order to test the validity of our model, we performed a calculation exactly like the one performed by Vitkova *et al.* We calculated the eccentricity of a vesicle and plot it as a function of the velocity of the vesicle as in Figure 3. Eccentricity is defined as $e = 2d/l$ where d and l where l is the length of the vesicles and d is the distance between the geometric and center of mass and are represented Figure 2. The results compare well as in both cases the vesicle asymptotically approaches the same maximal eccentricity of around 0.16. Vesicles which are less confined can tolerate higher velocities and experience a more gradual increase in eccentricity as velocity is increased. More mass is transferred to the rear of the vesicle as velocity increases and this leads to an increase in eccentricity. The shape of the vesicle as seen in Figure 3 is commonly known as a "bullet-shaped" vesicle. At low velocities, the vesicle shapes are more ellipsoidal than the shape represented in Figure 2 and have lower eccentricities.

Rather than expressing our velocities in units of σ/τ, it is useful to convert our units into a dimensionless form. The Vitkova *et al.* data have velocities which range from 0 to 1400 $\mu m/s$; converting our LJ-based units of velocity into SI units would yield velocities that are much greater than the Vitkova velocities. A L-J fluid presents a less viscous environment than water (a L-J fluid is more gas-like than fluid-like) therefore one might expect that higher velocities would be required to achieve the deformations in the Vitkova et al. experiment. So rather than expressing our velocities in SI units, they are expressed as dimensionless units of the "natural" velocity of the vesicle as defined by $V_0 = \kappa/\eta/R_0^2$ [4]. For typical experiments on vesicles such as in [2], $\eta_{water} \approx 1cP$, $\kappa \approx 20k_bT$, and $R_0 \approx 10\mu m$ and therefore $V_0 \approx 1\mu m/s$. Therefore, as an approximation, $V*$ in Figure 3 could be viewed as being in units of $\mu m/s$. Our vesicle is soft (with bending rigidity of $4k_bT$) and therefore small velocities in units of V_0 achieve the same deformations as the Vitkova experiment.

For the eccentricity results in Figure 3 we analyzed only steady-state shapes of vesicles. At higher velocities, the vesicles become unstable and likely to experience rupture. At high velocities the shapes are not stable and are prone to develop tether-like protrusions from the rear. At the same time they are also likely to suddenly burst at the front of the vesicle. To analyze why this is the case, we will look at the area expansion along the membrane as a function of the length of the vesicle.

1. *Membrane Tension and Rupture*

We calculate the average area per lipid head in a section of membrane as a function of the length of the vesicle

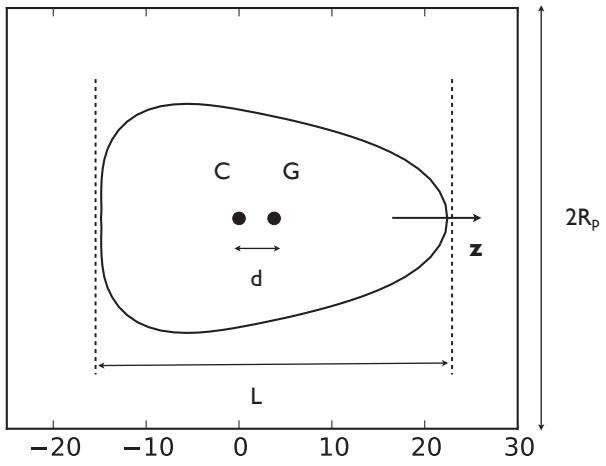

FIG. 2. A bullet-shaped vesicle for $\lambda = R_0/R_p = 0.6$. The center of mass of the vesicle is labelled by C and the geometric center is labelled as G. Eccentricity is defined as e=2d/l.

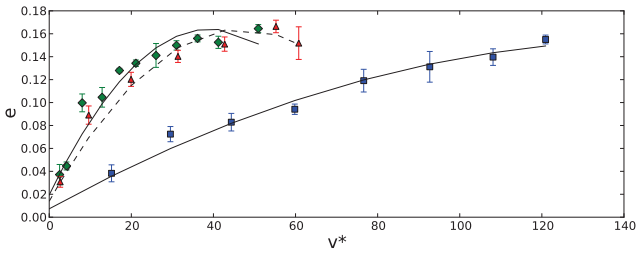

FIG. 3. Eccentricity of a vesicle versus velocity in dimensionless units of $V* = V/V_0$ for various confinements (where V is the velocity of the vesicle): ◆= 0.71, ▲= 0.67, and ■= 0.43. Lines are drawn through the points to guide the eye. This graphs corresponds well to reference [2].

as seen in Figure 4. We convert this to a dimensionless strain called α_{eff} where $\alpha_{eff} = (a_{avg} - a_0)/a_0$. For our initial spherical configuration of our vesicle, a_{avg} is less than a_0 due to the compression of the inner heads. $a_{avg,0} = (a_{0,+} + a_{0,-})/2 = 1.77\sigma^2$, but $a_0 \equiv 1.9\sigma^2$. Therefore α_{eff} for our initial configuration is less than zero and is expressed as the dashed line in Figure 4 to show the expansion with respect to the initial configuration. The point of rupture was determined by averaging of several rupturing vesicles from different simulations and is indicated on Figure 4 as a dot with error bars.

This analysis provides a good description of the build-up of tension in the membrane as the peak in tension corresponds well to the ultimate position of rupture as can be seen in Figure 4. The area expansion is greater for a highly confined vesicle ($\lambda = 1.0$) than it is for the least confined vesicle $\lambda = 0.6$ for the same capillary number.

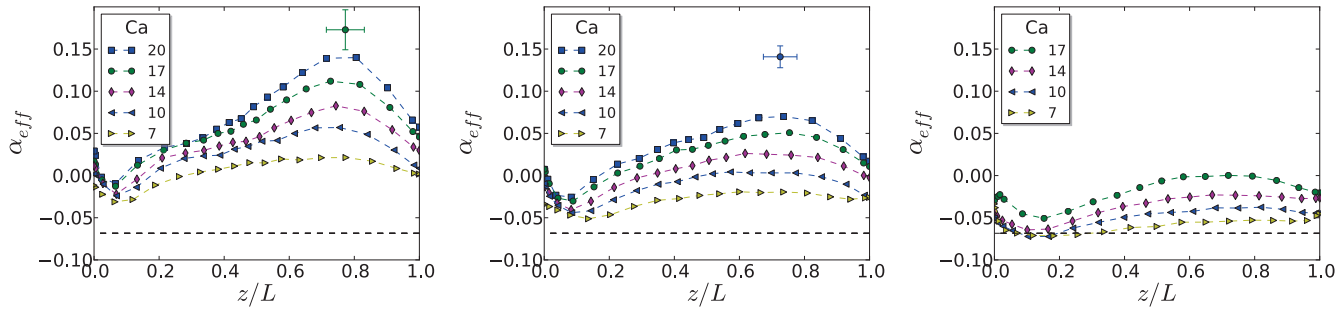

(a)$\lambda = 1.0$ (b)$\lambda = 0.8$ (c)$\lambda = 0.6$

FIG. 4. The effective area expansion along the membrane as a function of the length of the vesicle for different flow strengths (α_{eff} is the change in area with respect to an unstressed planar bilayer). There are clear points of rupture for the two more highly confined vesicles that occur where the effect of stretching is greatest; the approximate point of rupture with error is labeled on the graph. For $\lambda = 0.6$ the vesicle does not stretch much in flow and as such does not rupture like the two more confined vesicles. Instead as this vesicle becomes unstable it will develop a tether at the rear of the vesicle. The dotted line represents the area of the mid-plane of our vesicle as compared to a_0 for the initial configuration of the vesicle. With respect to a_0 the area per lipid on the mid-plane starts as compressed.

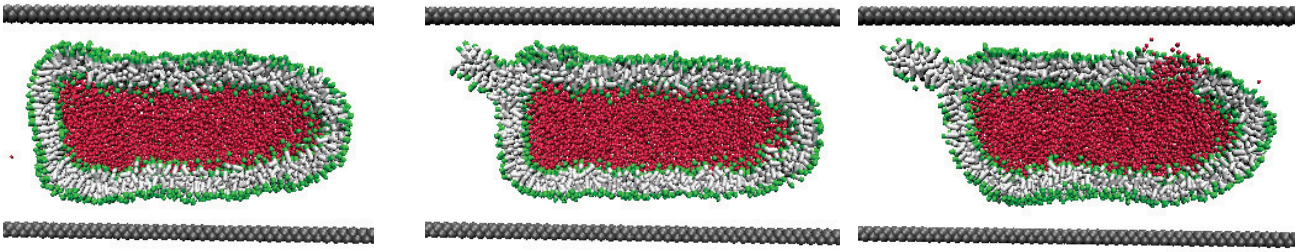

FIG. 5. The tether formation and rupture of a vesicle with $\lambda = 1.0$. At high capillary numbers, the vesicle starts as a stable shape and as the simulation time increases tethers will form at these high capillary numbers. In the last frame, the vesicle has ruptured and the internal contents are starting to leak out.

There is a build-up of tension near the front of the vesicle, but not quite at the tip. At the rear of the vesicle, the membrane is close to zero or negative tension. It would be expected that there is greater tension in the front cap of the vesicle as opposed to the back because of the pressure gradient along the channel [20]. The rear portion of the vesicle is unstable at the higher capillary numbers and is prone to developing tether-like protrusions as can be seen in Figures 5 and 6.

The stable configurations, as evidenced by their tension profiles in Figure 4, have significantly lower area expansions than at the time of rupture. Before a vesicle ruptures, there is a rapid stretching of the outer leaflet which results in tether formation and eventually rupture as can be seen in Figure 5. Vesicles with $\lambda = 0.8$ undergo even greater outer leaflet expansion that results in longer tethers than the vesicles with $\lambda = 1.0$. For our least confined vesicle, the tether falls from the main bulk of the vesicle before any bursting of the main part of the vesicle. The simulation can be considered unphysical at this point (as the tether can interact with the rest of the vesicle) and therefore no rupture of the vesicle is indicated on Figure 4.

At this point, it seems reasonable to ask whether tether formation would occur for micrometer-sized vesicles such are typically used in research. The fact that there is an asymmetry in the area per lipid of the inner and outer lipid heads is due the small-scale of our vesicle. This asymmetry leads to axial forces that can cause tether formation even in the absence of an external pulling force [21]. Tether formation occurs near the back of the vesicle where tension is close to zero. The asymmetry of the leaflets combined with the absence of tension could lead to tether formation. It would be interesting to see if this could be observed in larger vesicles in microfluidic devices in Poiseuille flow. However even for larger vesicles tether formation is known to happen as in the case vesicles in shear flow [22].

The capillary numbers from our simulation range from 0 to approximately 20. In the study by Farutin and Misbah [9], the range of capillary numbers from the fully inflated vesicles range from 0 to approximately 10 in

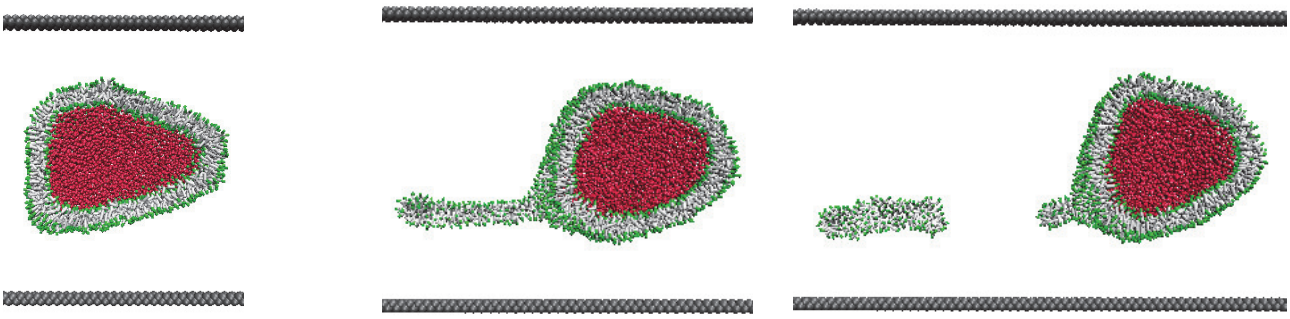

FIG. 6. Tether formation of a vesicle with $\lambda = 0.6$. As the tether lengthens, it will break off from the rest of the vesicle. The remaining bulk of the vesicle is vulnerable to rupture.

which they studied the shape deformation of vesicles in Poiseuille flow. As the flow strength increases, our vesicles become unstable. For all these pressure gradients, the force applied in the simulation was ramped at a constant rate. The most highly confined vesicles ($\lambda = 1.0$) can leak small amounts of its internal fluid as the pressure gradient increases at the higher capillary numbers ($\mathrm{Ca} \gtrapprox 17$).

The time scale for bending is much larger than the time scale of stretching. This was true in the Vitkova *et al.* experiment as well. As a vesicle both stretches and bends to minimize its free energy in flow, a vesicle can stretch very suddenly in response to any external change in flow stress before it can modify its shape. Sudden expansions in a membrane could lead to leakage. The release in tension of the membrane due to leakage can lead to the closing of pores. Such a phenomenon could explain minor leakage events that occur when a highly confined vesicle is subject to a small change in pressure gradient. Eventually, though there are pressure gradients for which a vesicle is unable to withstand and an event in which most of the inner fluid contents are lost will occur.

The tension as calculated by α_{eff} is mapped onto the vesicle surface as seen in Figure 7. In addition the velocity of the fluid in the vesicle's frame of reference is shown. The speed of the fluid gives an indication of the local forcing along the surface. Forces both normal and tangential to the surface contribute to the tension. The tangential force along the membrane is greatest along the sides of the vesicle where the velocity vectors are more parallel with the surface. This stress will be greatest near the front due to the cumulative elastic stretching along the sides. The normal forces also contribute to the surface tension in a Laplacian way. An an example, the velocity near the front of the least confined vesicle reduces the gauge pressure of the vesicle and will reduce the tension at the front tip.

Not shown by the fluid velocity is the pressure internal to the vesicle. The external pressure on the vesicle will be greatest at the tip and lessen toward the back due to the pressure gradient within the channel. There is an extra contribution to the external pressure due to the effect of the fluid flow around the vesicle; the fluid flow normal to the surface will impart an extra pressure to the vesicle. In the case of the least confined vesicle, the velocity of the fluid at the front will reduce the gauge pressure ΔP which will reduce the tension in the membrane in accordance with Laplace's pressure law.

An an experiment,a constant increase in the pressure gradient was applied until the vesicles ruptured. The dependence of rupture on capillary number is shown in Figure 8. Generally at higher confinements, vesicles break at lower capillary numbers but the variability in the data is large. Vesicles start to rupture around $\mathrm{Ca} \approx 24$ which is greater than the capillary number of ≈ 20 where they are still stable for significant amount of simulation time. The tension loading rate will affect at which capillary number the vesicle will rupture; a higher tension loading rate should cause higher mean tension which would lower the Ca* [14]. The tension loading rate chosen for this graph is the same tension loading rate applied to the vesicles that resulted in the tension profiles in Figure 4. If the force applied in the simulation is sudden, vesicles cannot handle pressure gradients as high as represented in Figure 8.

B. Deformation of vesicles with $\nu = 0.6$

We studied the deformation of vesicles with reduced volume $\nu = 0.6$ which is the same reduced volume as red bloods cells. It is of interest to examine the shape deformations of vesicles in order to compare with other modelling methods and to see how this may differ from RBC deformation under similar flow conditions. RBCs are more complex than vesicles and differ most notably in that they have a cytoskeleton which may limit extreme deformations [23]. Our shapes are plotted for a few different confinements and capillary numbers. This plot is very similar to the one done by Kaoui *et al.* in their modelling of 2D vesicles using BIM [6]. Our capillary numbers are as high as 20. Generally capillary numbers of 20 and above are of the range experienced by normal, healthy cells while lower capillary numbers would be ex-

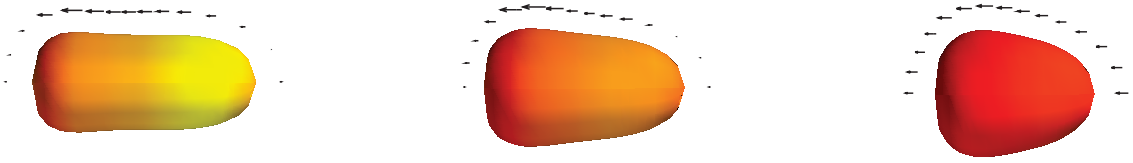

(a)$\lambda = 1.0$ (b)$\lambda = 0.8$ (c)$\lambda = 0.6$

FIG. 7. The lighter (yellow) color indicates the point of highest stress and the darker (red) color indicates low or negative tension. The length of the velocity vectors do not indicate the same velocity in all three cases; the length of the arrows were chosen for clarity.

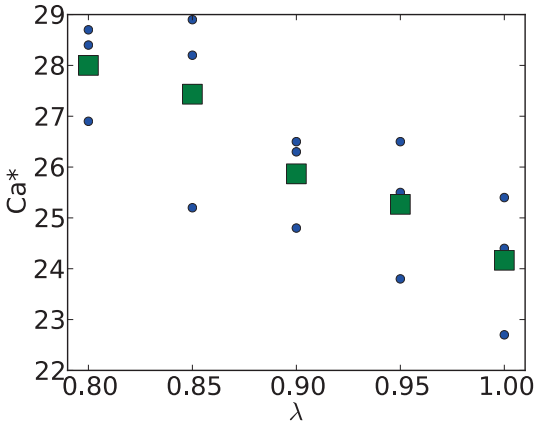

FIG. 8. The capillary numbers at which the vesicle will rupture, Ca*, as a function of confinement, λ. A constant, slow increase in pressure gradient was applied until the vesicle ruptured. The green squares represent the average capillary number while the blue dots represent the individual simulations.

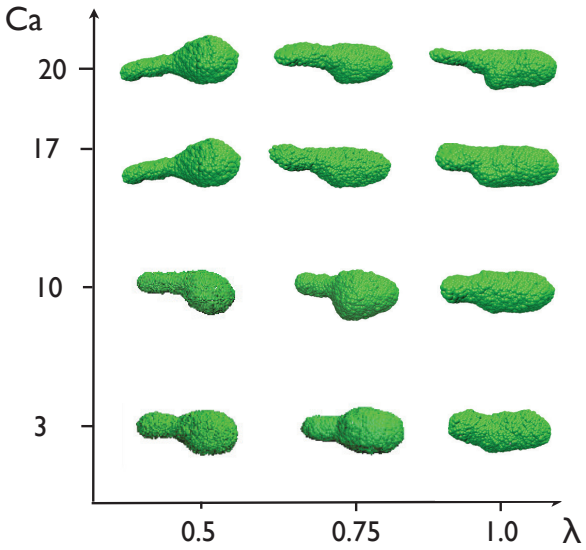

FIG. 9. Shape deformations of vesicles with $\nu = 0.6$ at different flow strengths and confinements. All of these shapes can be described as slipper-like. As capillary number increases, the "tails" of these slippers elongate. The tails of the vesicles at Ca $\geq$ 17 will eventually disconnect as the simulation time progresses. Although the force applied in the simulation is slowly ramped up to avoid sudden stresses, these vesicles are prone to leaking small amounts of inner content at the higher flow strengths as the force applied is increased. This figure shows good, but not perfect, agreement with reference [6].

pected for less deformable, unhealthy RBCs [6] .

For all the flow conditions illustrated in Figure 9 our vesicles show slipper-like configurations as their stable shape. Vesicles often start as parachute-like objects but then evolve into a non-axisymmetric slipper-like shape. At the higher capillary numbers the single "tails" of these slipper-like shapes become longer. At high forces, this tail will disconnect from the main body of the vesicle. This form of breaking is similar to the fully-inflated vesicles with a confinement of 0.6. The excess area of the outer leaflet "streams" in flow and forms a tether-like or tail-like object. The neck connecting the tail and the main bulk of the vesicle narrows to the point that the tail will detach often without leaking any interior content. Vesicles are unstable at Ca $\approx$ 20 and if the output of the simulations are run for long enough, these vesicles will break apart.

A notable result from Figure 9 may be the lack of any stable parachute-like vesicles. Kaoui *et al.* [6] find a stable parachute-like configuration for vesicles with confinement $\lambda = 0.5$ for the capillary number Ca $\gtrapprox$ 15, but we find a stable slipper-like vesicles at these flow strengths.

While Noguchi and Gompper find parachute and prolate ellipsoid shapes for vesicles with $\lambda = 0.7$ at moderate flow strengths [3]. It is generally excepted that in capillaries RBCs tend to adopt slipper-like shapes. Typical RBCs have a surface area of $\sim 135\mu m^2$ and therefore have a radius of an equivalent sphere of around $0.3\mu m$ [24]. The range of capillaries' radii is from 5 to 10 μm which results in typical confinements of $\lambda \sim 0.3$ to 0.6. So our slipper-like shape at $\lambda = 0.5$ is the shape typical of RBCs at that confinement.

V. DISCUSSION AND CONCLUSION

With our MD simulation, it is possible to expose our vesicles to shear forces great enough to tear the bilayer. This approach is different than other theoretical work in which the membrane is often assumed to have small area expansions and an impenetrable membrane. The tension profile of vesicles, as measured by the average area expansion of the outer and inner lipid heads, shows a peak stress point near the front tip of vesicles. The stress is greater for highly confined vesicles versus less confined vesicles, and can lead to rupture of the interior contents at high pressure gradients. Since our average area per lipid head starts as compressed (due to the scale of the vesicle), there appears to be a tendency for the excess area of the outer shell to "stream" in the flow and to form tether-like protrusions which can subsequently break off from the bulk of the vesicle. It would be interesting to see if the rupture of vesicles could be photographed in a microfluidic setup and if tether formation is observed.

We expressed the pressure gradient in the form a dimensionless capillary number. The capillary number is defined based on the vesicle's nominal radius, the bending modulus, and the pressure gradient. Our capillary numbers range from 0 to 20. However, this capillary number can span several decades. In the Vitkova *et al.* experiment, typical capillary numbers are around 1000. Coupier *et al.* studied vesicles with small excess area with capillary numbers as high as 10^4 [16]. Even though our fully-inflated vesicles have a smaller range capillary numbers than studies performed with Giant Unilamellar Vesicles (GUVs), the deformation of our vesicle does correspond with the deformations as measured by eccentricity when compared to experimental data.

Under a constant force ramp, higher confined vesicles will rupture before lesser confined vesicles. This is reasonable as the tension in the bilayer is greater overall at higher confinements for the same pressure gradient. For weaker confinements of $\lambda \approx 0.6$, our vesicles will develop and lose tethers before rupture. For a larger vesicles, such as GUVs, it is uncertain if tether formation would dominate over rupture as there would be less of an area difference between the two leaflets.

The simulation of vesicles in a capillary is very applicable to microfluidic setups in which small amounts or individuals particles can be manipulated under controlled conditions. A coarse-grained, molecular dynamics simulation could be an adjunct or alternative method for testing the response of cells or other particles in a particular microfluidic channels. The rupture of vesicles could be applicable to the fabrication of liposomes in microfluidic channels (in which a narrow distribution in size is desirable) as rupture is another method of limiting the size of liposomes.

For vesicles with reduced volume $\nu = 0.6$, we sampled the shape deformation of these vesicles for different capillary numbers and confinements. Our model has no constraints on the area expansion (beyond rupturing the membrane) which is different than many other methods which often assume limited area expansion of the membrane. Our vesicles are quite prone to large amounts of stretching in flow, but do attain stable slipper-like configurations at low and moderate forces. The length of our capillary is long compared to the vesicle and as such the vesicle occupies a small fraction of the fluid. Shape deformation of RBCs can be influenced by hematocrit volume fraction as RBCs packed into "trains" tend to exhibit parachute-like shapes [24]. In addition, shape deformation can be influenced by the properties of the capillary where stiffer capillaries (such as glass) will result in greater deformation than softer ones (such as microvasculature) [25]. These factors could lead to different results from our simulation than from other research such as Kaoui *et al.*. Modelling of vesicles with excess area continues to be an interesting area of research. It would be interesting to do a MD study in which a cytoskeleton-like polymer was attached to the bilayer and to observe the resulting change in shapes attained. This would add extra resistance to stretching to the bilayer and would perhaps increase the stability of the vesicle at large forces.

We studied how and why vesicles rupture in Poiseuille flow. The area expansion in the membrane is greatly increased with confinement and therefore highly-confined, fully-inflated vesicles rupture easily. The greatest concentration of force, while not at the front tip, is close to the front. There is zero to negative tension (as measured by the area expansion) at the rear of the vesicles. This appears to lead to instabilities that can result in tether-like protrusions.

We also presented results of the deformation of vesicles with reduced volume $\nu = 0.6$. These results can be compared to other studies that examine the dynamics of $\nu = 0.6$ vesicles or RBCs under flow. Our results are similar and a CGMD model with an explicit solvent provides another method in which to study these complicated dynamics.

[1] D. Lasic, Trends Biotechnol., **16**, 307 (1998), ISSN 01677799.

[2] V. Vitkova, M. Mader, and T. Podgorski, Europhys.

Lett., **68**, 398 (2004), ISSN 0295-5075.
[3] H. Noguchi and G. Gompper, Proc. Nat. Acad. Sci. U.S.A., **102**, 14159 (2005), ISSN 0027-8424.
[4] B. Kaoui, G. H. Ristow, I. Cantat, C. Misbah, and W. Zimmermann, Phys. Rev. E, **77**, 021903 (2008), ISSN 1539-3755.
[5] G. Danker, P. M. Vlahovska, and C. Misbah, Phys. Rev. Lett., **102**, 148102 (2009), ISSN 0031-9007.
[6] B. Kaoui, N. Tahiri, T. Biben, H. Ez-Zahraouy, A. Benyoussef, G. Biros, and C. Misbah, Phys. Rev. E, **84**, 1 (2011), ISSN 1539-3755.
[7] B. Kaoui, J. Harting, and C. Misbah, Phys. Rev. E, **83**, 1 (2011), ISSN 1539-3755.
[8] T. Biben, A. Farutin, and C. Misbah, Phys Rev E, **83**, 031921 (2011), ISSN 1539-3755.
[9] A. Farutin and C. Misbah, Phys. Rev. E, **011902**, 1 (2011).
[10] A. Farutin, O. Aouane, and C. Misbah, Phys. Rev. E, **85**, 061922 (2012), ISSN 1539-3755.
[11] W. Helfrich, Z. Naturforsch. c (1973).
[12] M. Idiart and Y. Levin, Phys. Rev. E, **69**, 061922 (2004), ISSN 1539-3755.
[13] L. Fournier and B. Joós, Phys. Rev. E, **67**, 051908 (2003), ISSN 1063-651X.
[14] P.-A. Boucher, B. Joós, M. J. Zuckermann, and L. Fournier, Biophys. J., **92**, 4344 (2007), ISSN 0006-3495.
[15] M. Bertrand and B. Joós, Phys Rev E, **85**, 051910 (2012), ISSN 1539-3755.
[16] G. Coupier, A. Farutin, C. Minetti, T. Podgorski, and C. Misbah, Phys. Rev. Lett., **108**, 178106 (2012), ISSN 0031-9007.
[17] N. Amenta, M. Bern, and M. Kamvysselis, ...of the 25th annual conference on ... (1998).
[18] R. Goetz and R. Lipowsky, J. Chem. Phys., **108**, 7397 (1998).
[19] S. J. Marrink and A. E. Mark, J. Am. Chem. Soc., **125**, 15233 (2003), ISSN 0002-7863.
[20] R. Bruinsma, Physica A: Stat. Theor. Phys., **234**, 249 (1996), ISSN 03784371.
[21] T. Powers, G. Huber, and R. Goldstein, Phys. Rev. E, **65**, 041901 (2002), ISSN 1063-651X.
[22] N. Shahidzadeh, D. Bonn, O. Aguerre-Chariol, and J. Meunier, Phys. Rev. E, **81**, 4268 (1998), ISSN 0031-9007.
[23] G. Lim H W, M. Wortis, and R. Mukhopadhyay, Proc. Nat. Acad. Sci. U.S.A., **99**, 16766 (2002), ISSN 0027-8424.
[24] S. Guido and G. Tomaiuolo, Comptes Rendus Physique, **10**, 751 (2009), ISSN 16310705.
[25] Y. Suzuki, N. Tateishi, M. Soutani, and N. Maeda, Microcirculation, **3**, 49 (1996), ISSN 1073-9688.

Bibliography

[1] HOOMD-blue web page: http://codeblue.umich.edu/hoomd-blue/.

[2] M. Abkarian. High-speed microfluidic differential manometer for cellular-scale hydrodynamics. *Proc. Nat. Acad. Sci. U.S.A.*, 103(3):538–542, January 2006.

[3] Manouk Abkarian, Magalie Faivre, Renita Horton, Kristian Smistrup, Catherine A Best-Popescu, and Howard A Stone. Cellular-scale hydrodynamics. *Biomed. Mater.*, 3(3):034011, September 2008.

[4] B. J. Alder and T. E. Wainwright. Phase Transition for a Hard Sphere System. *J. Chem. Phys.*, 27(5):1208, November 1957.

[5] Theresa M Allen and Pieter R Cullis. Drug delivery systems: entering the mainstream. *Science*, 303(5665):1818–22, March 2004.

[6] N Amenta, M Bern, and M Kamvysselis. A new Voronoi-based surface reconstruction algorithm. *SIGGRAPH '98*, 1998.

[7] Joshua a. Anderson, Chris D. Lorenz, and A. Travesset. General purpose molecular dynamics simulations fully implemented on graphics processing units. *J. Comput. Phys.*, 227(10):5342–5359, May 2008.

[8] M Bertrand. *Deformed soft matter under constraints*. PhD thesis, University of Ottawa, 2012.

[9] Martin Bertrand and Béla Joós. Extrusion of small vesicles through nanochannels: A model for experiments and molecular dynamics simulations. *Phys. Rev. E*, 85(5):051910, May 2012.

[10] Timo Betz, Martin Lenz, Jean-François Joanny, and Cécile Sykes. ATP-dependent mechanics of red blood cells. *Proc. Nat. Acad. Sci. U.S.A.*, 106(36):15320–5, September 2009.

[11] A-F Bitbol, L Peliti, and J-B Fournier. Membrane stress tensor in the presence of lipid density and composition inhomogeneities. *Eur. Phys. J. E*, 34(5):1–13, May 2011.

[12] Pierre-Alexandre Boucher, Béla Joós, Martin J Zuckermann, and Luc Fournier. Pore formation in a lipid bilayer under a tension ramp: modeling the distribution of rupture tensions. *Biophys. J.*, 92(12):4344–55, June 2007.

[13] Robijn Bruinsma. Rheology and shape transitions of vesicles under capillary flow. *Physica A: Stat. Theor. Phys.*, 234(1-2):249–270, December 1996.

[14] PB Canham. The minimum energy of bending as a possible explanation of the biconcave shape of the human red blood cell. *J. Theo. Biol.*, 1970.

[15] J Cotton and W Grant. Computational models of hair cell bundle mechanics: I. Single stereocilium. *Hearing Res.*, 2004.

[16] Gwennou Coupier, Alexander Farutin, Christophe Minetti, Thomas Podgorski, and Chaouqi Misbah. Shape Diagram of Vesicles in Poiseuille Flow. *Phys. Rev. Lett.*, 108(17):178106, April 2012.

[17] Gerrit Danker, Petia M Vlahovska, and Chaouqi Misbah. Vesicles in Poiseuille flow. *Phys. Rev. Lett.*, 102(14):148102, April 2009.

[18] E. Evans and W. Rawicz. Entropy-driven tension and bending elasticity in condensed-fluid membranes. *Phys. Rev. Lett.*, 64(17):2094–2097, April 1990.

[19] E. Evans and A. Yeung. Hidden dynamics in rapid changes of bilayer shape. *Chem. Phys. Lipids*, 73(1-2):39–56, September 1994.

[20] Alexander Farutin and Chaouqi Misbah. Symmetry breaking of vesicle shapes in Poiseuille flow. *Phys. Rev. E*, 011902(5588):1–7, 2011.

[21] J.-B. Fournier, N. Khalifat, N. Puff, and M. I. Angelova. Chemically Triggered Ejection of Membrane Tubules Controlled by Intermonolayer Friction. *Phys. Rev. Lett.*, 102(1):018102, January 2009.

[22] Luc Fournier and Béla Joós. Lattice model for the kinetics of rupture of fluid bilayer membranes. *Phys. Rev. E*, 67(5):051908, May 2003.

[23] R Goetz and Reinhard Lipowsky. Computer simulations of bilayer membranes: Self-assembly and interfacial tension. *J. Chem. Phys.*, 108(17):7397–7409, 1998.

[24] G Gregoriadis. Engineering liposomes for drug delivery: progress and problems. *Trends Biotechnol.*, 1995.

[25] G Gregoriadis. Engineering liposomes for drug delivery: progress and problems. *Trends in Biotechnol.*, 13(12):527–37, December 1995.

[26] Stefano Guido and Giovanna Tomaiuolo. Microconfined flow behavior of red blood cells in vitro. *C. R. Phys.*, 10(8):751–763, November 2009.

[27] W Helfrich. Elastic properties of lipid bilayers: theory and possible experiments. *Z. Naturforsch. c*, 1973.

[28] PJ Hoogerbrugge and J Koelman. Simulating microscopic hydrodynamic phenomena with dissipative particle dynamics. *Europhys. Lett.*, 1992.

[29] W Humphrey, A Dalke, and K Schulten. VMD: visual molecular dynamics. *J. Mol. Graph.*, 1996.

[30] Marco Idiart and Yan Levin. Rupture of a liposomal vesicle. *Phys. Rev. E*, 69(6):061922, June 2004.

[31] B. Kaoui, G. H. Ristow, I. Cantat, C. Misbah, and W. Zimmermann. Lateral migration of a two-dimensional vesicle in unbounded Poiseuille flow. *Phys. Rev. E*, 77(2):021903, February 2008.

[32] B. Kaoui, N. Tahiri, T. Biben, H. Ez-Zahraouy, A. Benyoussef, G. Biros, and C. Misbah. Complexity of vesicle microcirculation. *Phys. Rev. E*, 84(4):1–5, October 2011.

[33] Badr Kaoui, Alexander Farutin, and Chaouqi Misbah. Vesicles under simple shear flow: Elucidating the role of relevant control parameters. *Phys. Rev. E.*, 80(6):061905, December 2009.

[34] D Lasic. Novel applications of liposomes. *Trends Biotechnol.*, 16(7):307–321, July 1998.

[35] Philip R Leduc, Michael S Wong, Placid M Ferreira, Richard E Groff, Kiryn Haslinger, Michael P Koonce, Woo Y Lee, J Christopher Love, J Andrew McCammon, Nancy A Monteiro-Riviere, Vincent M Rotello, Gary W Rubloff, Robert Westervelt, and Minami Yoda. Towards an in vivo biologically inspired nanofactory. *Nat. Nanotechnol.*, 2(1):3–7, January 2007.

[36] Gerald Lim H W, Michael Wortis, and Ranjan Mukhopadhyay. Stomatocyte-discocyte-echinocyte sequence of the human red blood cell: evidence for the bilayer- couple hypothesis from membrane mechanics. *Proc. Nat. Acad. Sci. U.S.A.*, 99(26):16766–9, December 2002.

[37] HJ Limbach, A Arnold, BA Mann, and C Holm. ESPResSoan extensible simulation package for research on soft matter systems. *Comput. Phys. Commun.*, 2006.

[38] W Liu, B Schmidt, G Voss, and W Müller-Wittig. Molecular dynamics simulations on commodity GPUs with CUDA. *Lecture Notes in Computer Science*, 2007.

[39] Antonin Marchand, Joost H. Weijs, Jacco H. Snoeijer, and Bruno Andreotti. Why is surface tension a force parallel to the interface? *Am. J. Phys.*, 79(10):999, October 2011.

[40] Philippe Marmottant, Thierry Biben, and Sascha Hilgenfeldt. Deformation and rupture of lipid vesicles in the strong shear flow generated by ultrasound-driven microbubbles. *Proc. R. Soc. A*, 464(2095):1781–1800, July 2008.

[41] Siewert J Marrink and Alan E Mark. Molecular dynamics simulation of the formation, structure, and dynamics of small phospholipid vesicles. *J. Am. Chem. Soc.*, 125(49):15233–42, December 2003.

[42] Siewert J Marrink, H Jelger Risselada, Serge Yefimov, D Peter Tieleman, and Alex H de Vries. The MARTINI force field: coarse grained model for biomolecular simulations. *J. Phys. Chem. B*, 111(27):7812–24, July 2007.

[43] P Méléard, LA Bagatolli, and T Pott. Giant unilamellar vesicle electroformation: From lipid mixtures to native membranes under physiological conditions. *Method. Enyzmol.*, 2009.

[44] P Nelson. *Biological Physics (Updated Edition)*. WH Freeman, 2007.

[45] Hiroshi Noguchi and Gerhard Gompper. Shape transitions of fluid vesicles and red blood cells in capillary flows. *Proc. Nat. Acad. Sci. U.S.A.*, 102(40):14159–64, October 2005.

[46] Vincent Noireaux and Albert Libchaber. A vesicle bioreactor as a step toward an artificial cell assembly. *Proc. Nat. Acad. Sci. U.S.A.*, 101(51):17669–74, December 2004.

[47] S Nosé. A molecular dynamics method for simulations in the canonical ensemble. *Mol. Phys.*, 1984.

[48] RB Phillips, J Kondev, J Theriot, N Orme, and H Garcia. *Physical biology of the cell*. Garland Science, 2009.

[49] Thomas Powers, Greg Huber, and Raymond Goldstein. Fluid-membrane tethers: Minimal surfaces and elastic boundary layers. *Phys. Rev. E*, 65(4):041901, March 2002.

[50] N Sciaky, J Presley, C Smith, K J Zaal, N Cole, J E Moreira, M Terasaki, E Siggia, and J Lippincott-Schwartz. Golgi tubule traffic and the effects of brefeldin A visualized in living cells. *J. Cell Bio.*, 139(5):1137–55, December 1997.

[51] Udo Seifert. Configurations of fluid membranes and vesicles. *Adv. Phys.*, 46(1):13–137, February 1997.

[52] Noushine Shahidzadeh, Daniel Bonn, Olivier Aguerre-Chariol, and Jacques Meunier. Large Deformations of Giant Floppy Vesicles in Shear Flow. *Phys. Rev. E*, 81(19):4268–4271, November 1998.

[53] J Sinha, N Das, and M.K Basu. Liposomal antioxidants in combating ischemia-reperfusion injury in rat brain. *Biomed. Pharmacother.*, 55(5):264–271, June 2001.

[54] R. Skalak and P I Branemark. Deformation of Red Blood Cells in Capillaries. *Science*, 164(3880):717–719, May 1969.

[55] Thomas Soddemann, Burkhard Dünweg, and Kurt Kremer. Dissipative particle dynamics: a useful thermostat for equilibrium and nonequilibrium molecular dynamics simulations. *Phys. Rev. E*, 68(4 Pt 2), 2003.

[56] EM Toose, BJ Geurts, and JGM Kuerten. A boundary integral method for two-dimensional (non)-Newtonian drops in slow viscous flow. *J. Non-Newton. Fluids*, 1995.

[57] D D Verma, T S Levchenko, E A Bernstein, and V P Torchilin. ATP-loaded liposomes effectively protect mechanical functions of the myocardium from global ischemia in an isolated rat heart model. *J. Control Release*, 108(2-3):460–71, November 2005.

[58] V Vitkova, M Mader, and T Podgorski. Deformation of vesicles flowing through capillaries. *Europhys. Lett.*, 68(3):398–404, November 2004.

[59] Petia M. Vlahovska, Thomas Podgorski, and Chaouqi Misbah. Vesicles and red blood cells in flow: From individual dynamics to rheology. *C. R. Phys.*, 10(8):775–789, November 2009.

[60] FM White. Fluid Mechanics,(2003). *McGraw-Hill*, 2003.

[61] Masayuki Yokota, Eiichi Tani, Satoshi Tsubuki, Ikuya Yamaura, Ikuko Nakagaki, Seiki Hori, and Takaomi C Saido. Calpain inhibitor entrapped in liposome rescues ischemic neuronal damage. *Brain Res.*, 819(1-2):8–14, February 1999.

[62] Hernan Zhou, Beatriz Burrola Gabilondo, Wolfgang Losert, and Willem van de Water. Stretching and relaxation of vesicles. *Phys. Rev. E*, 83(1):011905, January 2011.